의학박사 학위논문

Effect of Periostin on Renal Fibrosis and Renal Function Deterioration

페리오스틴이 신섬유화와 신기능 저하에 미치는 영향

2017년 8월

서울대학교 대학원

의학과 내과학 전공

황 진 호

의학박사 학위논문

Effect of Periostin on Renal Fibrosis and Renal Function Deterioration

페리오스틴이 신섬유화와 신기능 저하에 미치는 영향

2017년 8월

서울대학교 대학원

의학과 내과학 전공

황 진 호

Effect of Periostin on Renal Fibrosis and Renal Function Deterioration

페리오스틴이 신섬유화와 신기능 저하에 미치는 영향

지도교수 임 춘 수

이 논문을 내과학 박사 학위논문으로 제출함

2017년 7월

서울대학교 대학원

의학과 내과학 전공

황 진 호

황진호의 박사 학위논문을 인준함

2017년 6월

위 원 장 (인)

부 위 원 장 (인)

위 원 (인)

위 원 (인)

위 원 (인)

Abstract

Effect of Periostin on Renal Fibrosis and Renal Function Deterioration

Jin Ho Hwang

Department of Medicine, Internal Medicine Major

The Graduate School

Seoul National University

Background: Periostin is a matricellular protein and plays a vital role in tissue regeneration, fibrosis, and wound healing via its interaction with integrin. Recently, the role of periostin has been explored in the field of nephrology. We investigated the role of periostin, the effect of periostin blockade in renal fibrogenesis, and its clinical significance including renal histologic findings and prognosis in IgA nephropathy (IgAN).

Methods: We investigated the function of periostin *in vivo* in wild-type and periostin-deficient mice (POSTN-KO) in a unilateral ureteral obstruction (UUO) model. For the *in vitro* experiments, primary cultured inner medullary collecting duct (IMCD) cells from the wild-type and POSTN-KO mice were used. For an experiment involving human, serum and urine periostin were measured in 314 IgA nephropathy patients using ELISA. The patients were divided into 3 groups by urine periostin/creatinine (uPOSTN/Cr): group 1 (undetectable), group 2 (lower than the median), and

group 3 (higher than the median).

Results: Periostin expression was strongly induced by the UUO in the wild-type mice. *In vitro*, the administration of recombinant TGF-β increased periostin expression in the wild-type IMCD cells. The effect of periostin blockade was examined by three ways. Compared to the wild-type mice, the POSTN-KO mice showed a more preserved kidney structure and less fibrous tissues. Fibrosis-related genes and the mRNA expression levels of inflammatory cytokines were increased in the wild-type mice and were significantly decreased in the POSTN-KO mice. The integrin blockade peptide and anti-periostin polyclonal antibody decreased the fibrosis-related gene expression. The uPOSTN/Cr level was correlated with pathologic classifications and both initial and final IDMS-MDRD eGFRs (P<0.001). Histologically, group 3 patients were correlated with severe interstitial fibrosis/tubular atrophy (P=0.004), interstitial inflammation (P=0.007), hyaline arteriolosclerosis (P=0.001), and glomerular sclerosis (P<0.001). A higher initial uPOSTN/Cr level was associated with a greater decline in eGFR during follow-up (P=0.043 when initial eGFR $\geq$ 60; P=0.025 when eGFR < 60 mL/min/1.73 m^2), and the renal outcomes with ESRD (P=0.003), ESRD and/or eGFR decrease of > 30% (P=0.033), and ESRD and/or eGFR decrease of > 50% (P=0.046) occurred significantly more in group 3. In multivariate analysis, uPOSTN group 3 (HR, 2.839; CI, 1.013-7.957; P=0.047) was independently associated with ESRD in IgAN patients.

Conclusion: Periostin is one of the markers of renal fibrosis and may augment the progression of fibrogenesis as an extracellular matrix protein.

Periostin blockade attenuated renal fibrogenesis via inhibiting the TGF-β signaling pathway, inflammation, and apoptosis. Urine POSTN/Cr value at initial diagnosis correlated with renal fibrosis and predicted the renal outcomes in patients with IgAN. Thus, periostin could be a promising urinary biomarker for renal fibrosis and periostin inhibition may be a therapeutic target for the amelioration of renal disease progression.

Keywords: Anti-periostin antibody; Biomarker; Chronic kidney disease; Fibrosis; IgA nephropathy; Periostin

***Student Number*:** 2012-30537

목 차

List of Tables

List of Figures

INTRODUCTION

Chronic kidney disease (CKD) causes irreparable and progressive renal damage. Various chronic diseases such as diabetes mellitus, hypertension, and glomerulonephritis cause CKD. Pathologically, renal fibrosis is a final common pathway for CKD, and tubulointerstitial fibrosis drives the progression of CKD to end-stage renal disease.[1-4] There an increased risk of morbidity and mortality in CKD patients,[5] and CKD contributes to an economic burden for the national healthcare system. Despite decades of extensive research, no specific treatments are available to prevent or reverse renal fibrosis.

Kidney fibrosis is the result of a failed healing process after an insult. Various intracellular signaling pathways are associated with kidney fibrosis, and transforming growth factor-β (TGF-β) plays a key role by modulating cell migration, inflammatory cell infiltration, and extracellular matrix (ECM) turnover.[6,7]

Periostin is a matricellular protein that is responsible for tissue regeneration, fibrosis, and wound healing by interacting with integrin.[8] Extensive investigations have been conducted in various neoplasms, asthma, and cardiac diseases.[9-12] Recently, the role of periostin has been emerging in the field of nephrology.[13-19] One of the studies showed that the inhibition of periostin expression was associated with decreased renal inflammation and fibrosis both *in vitro* and *in vivo*.[19]

IgA nephropathy (IgAN) is one of the most common forms of glomerulonephritis and a frequent cause of end-stage renal disease (ESRD)

worldwide.[20] In Korea, it accounts for approximately half of all primary glomerulonephritis.[21] IgAN represents various clinical features, from lifelong mild hematuria with or without proteinuria to rapid decline or loss of renal function after diagnosis. The prognosis of IgAN is unclear because of the lack of renal biopsy data of suspicious cases of IgAN with a clinically mild disease course and the low accuracy of diagnosis.[22] In one study on biopsy-proven IgAN population in Korea, ESRD occurred in 20.6% of patients and the median time to ESRD was 71 months after renal biopsy.[23] Owing to the heterogeneity of reports of disease course and clinical features of IgAN, reliably predicting outcome at diagnosis is difficult. Therefore, the development of noninvasive biomarkers with high sensitivity and specificity that can be used for predicting disease prognosis would be highly beneficial. Urinary biomarkers have several advantages; they could be collected in large volumes using noninvasive methods, and they are stable owing to the lack of endogenous proteases.[24]

We investigated the role of periostin *in vitro* using primary cultured inner medullary collecting duct (IMCD) cells and the effect of periostin blockade on renal fibrogenesis *in vivo* using periostin-deficient mice (POSTN-KO) and a polyclonal antibody against periostin. Also, the correlation between urinary periostin excretion and its clinical significance, including renal histologic findings in IgAN were evaluated.

METHODS

Experimental Animals and Unilateral Ureter Obstruction Model Establishment

This animal study was conducted at the Seoul Metropolitan Government Seoul National University Boramae Medical Center (SMG-SNU) and approved by the SMG-SNU Institutional Animal Care and Use Committee for compliance with regulations. The strain of periostin null mice (B6;*Postn*^{tm1Jmol}/J) was donated by Dong-Gu Hur, who originally purchased these mice from The Jackson Laboratory (Bar Harbor, Maine, USA).[25] C57BL/6 (WT) mice were purchased from the Korean SPF Laboratory Animal Company, KOATECH (Kyeonggi, Korea). To evaluate the knock-out effect of periostin on renal fibrosis, 7-8-week-old male C57BL/6 mice and POSTN-KO mice (weight 24.2 g for the WT mice and 19.4 g for the POSTN-KO mice) were randomly divided into four groups, which consisted of sham groups (1-week and 2-week models) and unilateral ureter obstruction (UUO) groups (1-week and 2-week models). The UUO operation was performed under anesthesia with intraperitoneal xylazine (Rompun; 10 mg/kg of body weight; Bayer, Canada) and tiletamine mixed with zolazepam (1:1) (Zoletil^{TM}; 30 mg/kg of body weight; Virbac, USA). After the left flank incisions, the UUO was achieved by ligating the left ureter with 5-0 silk at two points and cutting between the ligatures. The mice were placed on a heating pad (37°C), and pre-warmed PBS (37°C) was intraperitoneally administered throughout the procedure to the prevent dehydration. The

sham-operated mice underwent identical surgical procedures except for the ligation of the ureter. After 7 or 14 days, the mice were sacrificed, and the UUO left kidneys were collected for further analyses, including frozen section, immunohistochemistry (IHC), protein extraction, and RNA extraction. Three to five mice were used from each group, and three or four independent experiments were performed for each procedure.

Evaluation of Renal Histology

Formalin-fixed, paraffin-embedded tissues were cut into 4-μm sections. Fibrosis was assessed in similar tissue sections stained with Sirius Red and Masson's Trichrome.[26] Five to seven fields were selected randomly from each kidney, and the red-stained area per total area, which reflected the interstitial fibrosis, was quantified using computer-based morphometric analysis software (Qwin 3, Leica, Mannheim, Germany). Scoring was performed in a blinded manner. The data are expressed as the mean values of the percentage of the positive area examined.

Immunohistochemistry Analyses

Four-micron sections of formalin-fixed, paraffin-embedded tissue were deparaffinized and rehydrated using xylene and ethanol. Endogenous streptavidin activity was blocked using 3% hydrogen peroxide. The sections were probed with primary antibodies, followed by counterstaining with Mayer's hematoxylin (Sigma-Aldrich). The degree of nonspecific staining was evaluated using secondary antibodies and isotype control IgGs. To

examine the expression of human periostin and type I alpha 1 collagen (col Iα1), the staining was performed using polyclonal periostin and type I collagen antibodies (Abcam, Cambridge, MA) and incubating overnight at 4°C, followed by incubation with dextran polymer conjugated with horseradish peroxidase (HRP; DAKO, Carpintería, CA) for 40 minutes at room temperature. 3, 3'-diaminobenzidine tetrahydrochloride (Sigma-Aldrich, Saint Louis, MO) was used for the immunohistochemical detection. The stained slides were photographed under an Olympus inverted microscope (Olympus Imaging America, Center Valley, CA). For the evaluation of the human biopsy slides, every obtainable, unstained slide from the study population was used.

Immunofluorescence Staining and Confocal Microscopic Examination

For the immunofluorescence staining of the kidney tissues, deparaffinized sections of mouse specimens were probed with primary antibodies in a blocking agent overnight at 4°C, followed by an incubation with Alexa Fluor-conjugated secondary antibodies (Molecular Probes, Eugene, OR). 4', 6-Diamidino-2-phenylindole (DAPI; Molecular Probes) was used for the counterstaining. For the negative controls, the primary antibodies were omitted. Apoptosis was estimated by detecting the fragmented chromosomal DNA using the terminal deoxynucleotidyl transferase dUTP nick end labeling (TUNEL; Roche, Mannheim, Germany) assay according to the manufacturer's instructions. Confocal microscopy was performed with a Leica TCS SP8 STED CW (Leica).

Cell Culture

Primary cultured IMCD cells were used in this research study and identified by aquaporin-2 expression.[27] To maintain the best cell quality, each cell was used in only one generation, and we did not perform a subculture in the other experiments. All the cells were cultured at 37°C in an atmosphere of 21% oxygen and 5% carbon dioxide in Dulbecco's Modified Eagle's Medium/F-12 1:1 mixture with 10 mM D-glucose, 10% fetal bovine serum, 100 U/mL penicillin, 100 mg/mL streptomycin, and 2 mM supplemental glutamine (Gibco™,Thermo Fisher Scientific). The cells were grown to approximately 80% confluence and subjected to serum deprivation (1% FBS) for 24 hours before the application of the experimental cell treatment.

Administration of Recombinant POSTN, RGDS and Anti-Periostin Polyclonal Antibody

To confirm that the administration of recombinant POSTN (rPOSTN; R&D systems, Minneapolis, MN, USA) changes the morphology of the renal cells and exacerbates the renal fibrosis process, the primary cultured IMCD cells were treated with 5 ng/mL recombinant TGF-β (rTGF-β; positive control, R&D systems), 1.0 μg/mL rPOSTN (R&D systems), or both. Integrin blockade was performed by administering 250 μg/mL of a highly selective integrin receptor blocker, the RGDS peptide (Sigma-Aldrich), with rTGF-β + rPOSTN or rPOSTN alone for 72 hours to both the WT and POSTN-KO mice. The doses of the reagents were determined by examining each of

dose dependent effect and toxicity. To evaluate the effect of the periostin blockade, 1.0 μg of the anti-POSTNpab (R&D systems) was administered with 1.0 μg of rPOSTN. All agents were diluted in the cell culture media, and all *in vitro* experiments were repeated 3 times to confirm the reproducibility. The effect of the periostin blockade was also evaluated in an *in vivo* experiment. WT mice (7-8 weeks of age) were divided into 4 groups as follows: a sham group, a sham group treated with an isotype IgG, a UUO group, and a UUO group treated with anti-POSTN polyclonal antibody (aPOSTNab). The anti-POSTNab or isotype IgG (sham injection) was injected via the tail vein on 4 separate days following the UUO (day 0, 2, 4, and 6, with 40 μg, 20 μg, 20 μg, and 20 μg, respectively).

Analysis of mRNA Expression using Quantitative RT-PCR

Total RNA was isolated from the cells and renal tissues using the RNeasy® Kit (Qiagen GmBH, Hilden, Germany), and 1 μg of total RNA was reverse-transcribed using oligo-d(T) primers and AMV-RT Taq polymerase (Promega, Madison, WI, USA). The quantitative RT-PCR was performed using assay-on-demand TaqMan® probes and primers for Col Iα1, fibronectin, periostin, TGF-β, α-smooth muscle actin (αSMA), fibroblast-specific protein-1 (FSP-1), Integrin αv, β3, β5, focal adhesion kinase (FAK), integrin-linked kinase (ILK), monocyte chemoattractant protein-1 (MCP-1), interferon-ɣ (IFN-ɣ), interleukin-6 (IL-6), p53, Bcl-2, and glyceraldehyde 3-phosphate dehydrogenase (GAPDH) (Applied Biosystems, Foster City, CA) and an ABI PRISM® 7500 Sequence Detection System (Applied Biosystems). The thermocycler conditions were as follows: 95°C

for 10 minutes followed by 40 cycles of dissociation (95°C for 10 s), annealing (55°C for 30 s), and elongation (72°C for 30 s). The levels of the specific messenger RNA (mRNA) expression were normalized to the level of the GAPDH mRNA expression. The relative quantification was performed using the $2^{-\Delta\Delta CT}$ method.[28]

Western Blot Analysis

The protein samples (80 μg each) were separately subjected to 8-12% sodium dodecyl sulfate-polyacrylamide gel electrophoresis and transferred onto an Immobilon polyvinylidene difluoride membrane (Merck Millipore, Billerica, MA, USA) using a wet blotting apparatus (Bio-Rad, Hercules, CA, USA). The membranes were incubated for at least 1 hour in the blocking buffer (Tris-buffered saline, 0.05% Tween-20, and 5% bovine serum albumin or 5% nonfat milk), followed by an overnight incubation with the following primary antibodies at 4°C: αSMA (1:300, Abcam), FSP-1 (1:200, Abcam), fibronectin (1:50, Abcam), type I collagen (1:800, Abcam), and monoclonal mouse anti-β-actin (1:20000, Sigma-Aldrich, St. Louis, MO, USA). The membrane was then washed 4 times for 10 minutes with tris-buffered saline and Tween-20. The membrane was then incubated in a blocking buffer containing HRP-linked goat anti-mouse IgG (1:6,000 for β-actin; Cell Signaling Technology) or goat anti-rabbit IgG (1:5,000 for other primary antibodies; Cell Signaling Technology, Danvers, MA). After the repeated washing, the membrane was developed with the Amersham ECL chemiluminescence detection reagent (GE healthcare, Chicago, IL, USA). Quantifying the western blots was performed using Image J

(https://imagej.nih.gov/ij/).

Human Sample Study Design and Population

We included patients who underwent kidney biopsy at Seoul National University Hospital and SMG-SNU. These two centers are building the prospective cohorts and managing biobanks for urine, plasma, serum, genomic DNA, and biopsied tissue of all patients who underwent renal biopsy and provided informed consent.

We collected data of 399 adult patients with biopsy-proven IgAN from January 2009 to December 2014. We excluded 54 patients owing to non-availability of urine or plasma samples, insufficient follow-up or clinical data within 3 months of kidney biopsy (52 patients), and misdiagnosis (2 patients). Finally, 345 IgAN patients were included. In addition, 56 patients were randomly selected from the Seoul National University Boramae Medical Center Human Biobank for comparison with IgAN patients.

Clinical parameter data including age, sex, body mass index, blood chemistry, spot urine protein-creatinine ratio (uPCr), and comorbidity (hypertension, diabetes mellitus, and viral hepatitis) were collected at the time of kidney biopsy. Information on blood chemistry, uPCr, and prescribed medications (angiotensin-converting enzyme inhibitors or angiotensin II receptor blockers, and immunosuppressive agents) was recorded during the follow-up period. Estimated glomerular filtration rate (eGFR) was calculated using the isotope dilution mass spectrometry‐traceable modified Modification of Diet in Renal Disease equation. Biopsy tissues were examined using light, electron, and immunofluorescence microscopy. The

histologic diagnosis was made by a renal pathologist. Interstitial fibrosis and tubular atrophy (IFTA) and interstitial inflammation scores were graded as a percentage of affected area as follows: 0 (none), 1 (mild, ≤ 25%), 2 (moderate, 26%-50%), and 3 (severe, > 50%). Information on fibrointimal thickening and hyaline arteriolosclerosis was obtained by final pathologic record of each patient. This study was approved by the Institutional Review Board (H-1308-120-517), and the patients provided informed consent prior to recruitment into the cohort. All clinical investigations were conducted in accordance with the guidelines of the 2013 Declaration of Helsinki.

Measurement of Tissue, Urine, and Plasma Periostin Levels

The mice kidneys were harvested and prepared for the protein extraction. The capsule of the kidney was removed, and the kidney tissue was stored at -80°C. The tissues were homogenized (Biospec products, Bartlesville, OK, USA) with 500 µL of lysis buffer (Radio-immunoprecipitation assay buffer with 0.005 M Ethylenediamine-tetraacetic acid, protease inhibitor cocktail, and 0.001 M phenylmethane sulfonyl fluoride). The mixture was incubated for 10 minutes at room temperature and then centrifuged at 14,000 rpm at 4°C for 20 minutes. The supernatant was aliquoted to a new tube and quantified using the bicinchoninic acid assay (Pierce™ BCA Protein Assay Kit, Thermo Scientific, Waltham, MA, USA). All samples were adjusted to a concentration of 2 mg/mL. The tissue, urine, and plasma periostin levels were measured using an enzyme-linked immunosorbent assay (ELISA; R&D systems, Minneapolis, MN, USA) according to the manufacturer-provided protocol. Ninety-six-well microplates were coated with 1 µg/mL, 100 µL per

well of the mouse anti-periostin antibody (capture antibody) and incubated overnight at room temperature. The plates were washed three times with a wash buffer (0.05% Tween-20 in phosphate buffered saline) and blocked with the reagent diluent for more than 1 hour. Subsequently, 100 μL of all standards and samples were added to each well and incubated for 2 hours at room temperature. After 2-hour incubation with the detection antibody, a 20-min incubation with streptavidin-HRP, and a 20-min incubation with the substrate solution, the stop solution was added to each well. The periostin absorbance was calculated at 450 nm by correcting for the plate artifact at 570 nm and using a 4-parameter logistic standard curve. All measurements were performed in a blind manner and duplicated. The tissue and plasma samples were diluted to 1:50 before the sample loading. Measured urine periostin levels were adjusted by urine creatinine. Urine creatinine concentrations were measured in the same urine samples, and expressed as the urine periostin/creatinine ratio (uPOSTN/Cr).

Grouping and Outcomes

We divided the patients into 3 groups by uPOSTN/Cr: group 1 (undetectable level of uPOSTN); group 2 (below median value of measured uPOSTN/Cr); and group 3 (above median value of measured uPOSTN/Cr). We also evaluated the patients with plasma POSTN by quartile groups.

Renal outcomes were compared between the low uPOSTN group (group 1 and 2) and group 3. The occurrence of ESRD was the primary outcome in this study. An eGFR decrease $\geq$ 30% and/or ESRD, and eGFR decrease $\geq$ 50% and/or ESRD were secondary outcomes. The change in

eGFR per year (ΔeGFR/year) was also evaluated by collecting final follow-up data and assessing the duration of total follow-up. We evaluated the association between uPOSTN/Cr and pathological parameters.

Statistical Analysis

Most analyses and calculations were performed using Prism® version 6 (GraphPad Software, La Jolla, Ca, USA) and IBM SPSS Statistics V21.0 (IBM Corporation, Armonk, NY, USA). Continuous variables were expressed as the mean ± standard deviation and categorical variables as the number and percentage. The independent samples *t*-test was used for continuous variables. For multiple comparisons, one-way analysis of variance was used followed by the least significant difference test. Categorical data were compared using the chi-square test. Pearson correlation coefficients were determined to explore the relationship between urine periostin and plasma periostin, initial eGFR, and uPCr. The ESRD-free survival rates and other event-free survival rates were calculated using the Kaplan-Meier method, and comparison between groups was performed using the log-rank test. The Cox regression model was used to identify independent risk factors for ESRD, and to calculate the HR and 95% CI. Finally, receiver operating characteristics (ROC) analysis was used to calculate the area under the curve (AUC) for uPOSTN/Cr level and to find the best cut-off value to predict the outcome of ESRD. The *in vitro* and *in vivo* study results were analyzed using the Kruskal-Wallis nonparametric test for multiple comparisons. The ROC analysis was performed using R version 3.2.0 (R Foundation for Statistical Computing, Wien, Austria). Statistical significance was determined

at $P < 0.05$. The P-values are represented as * $P < 0.05$, ** $P < 0.01$, and *** $P < 0.001$ for all comparisons.

RESULTS

Expression of Periostin and Fibrosis-Related Markers in a Unilateral Ureteral Obstruction model in Wild-Type and Periostin-Deficient Mice

To identify the role of periostin, we performed UUO operation in both WT mice and POSTN-KO mice. The gross appearance of the mouse kidney 1 week and 2 weeks after the UUO is shown in Figure 1. At 1 week and 2 weeks after the UUO, an increase in Col Iα1 and a decrease in the renal mass were detected. The IHC assay results showed that the expression of type I collagen and periostin were strongly induced 1 week after the UUO and became more pronounced 2 weeks after the UUO. The extent of the renal fibrosis after the UUO was significantly lower in the POSTN-KO mice than in the WT mice. In the morphometric analysis, the collagen positive area was significantly increased in the WT mice ($P < 0.001$), and the POSTN-KO mice showed less fibrous tissue ($P < 0.05$) in the UUO 1-week model than the WT mice ($P < 0.001$ for others) (Figure 2A).

Fibrosis-related genes, such as Col Iα1, fibronectin, αSMA, and FSP-1 mRNA, were increased in the wild-type mice ($P < 0.001$) and were significantly decreased in the periostin KO mice ($P < 0.05$ for Col Iα1 and fibronectin; $P < 0.01$ for αSMA; and $P < 0.001$ for FSP-1). Additionally, TGF-β expression was strongly induced by the fibrosis-related markers (Figure 2B). The expression of the fibrosis-related genes was more

prominently increased 2 weeks after the UUO (Figure 3). Although the gene expression differences between the WT mice and the POSTN-KO mice were intense, the αSMA protein levels showed a pattern that was similar to that observed in previous results (Figure 2C). To determine whether periostin could play a role as a fibrosis marker, we examined periostin mRNA expression and verified the upregulation of periostin, which was accompanied by the upregulation of other fibrosis-related genes ($P < 0.001$). Moreover, the periostin protein levels were markedly increased in the UUO mice compared to those in the sham mice (Figure 2D). In summary, periostin and the fibrosis-related markers are highly induced in the kidneys by the UUO model and were attenuated in the POSTN-KO mice.

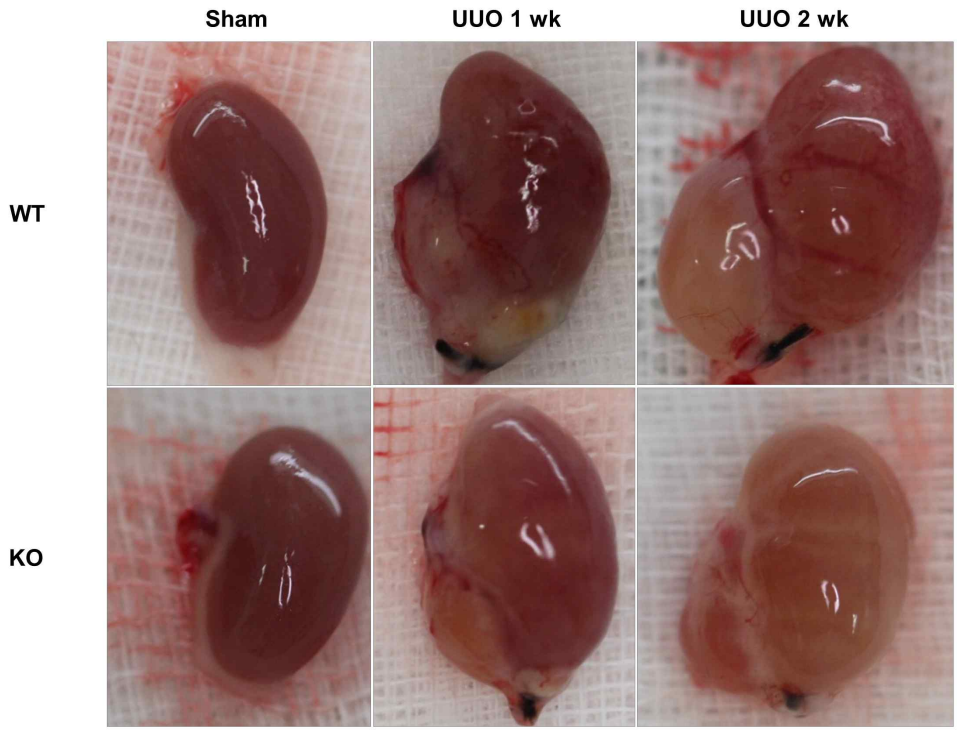

Figure 1. Gross appearance of the mouse kidney at 1 week and 2 weeks after the UUO

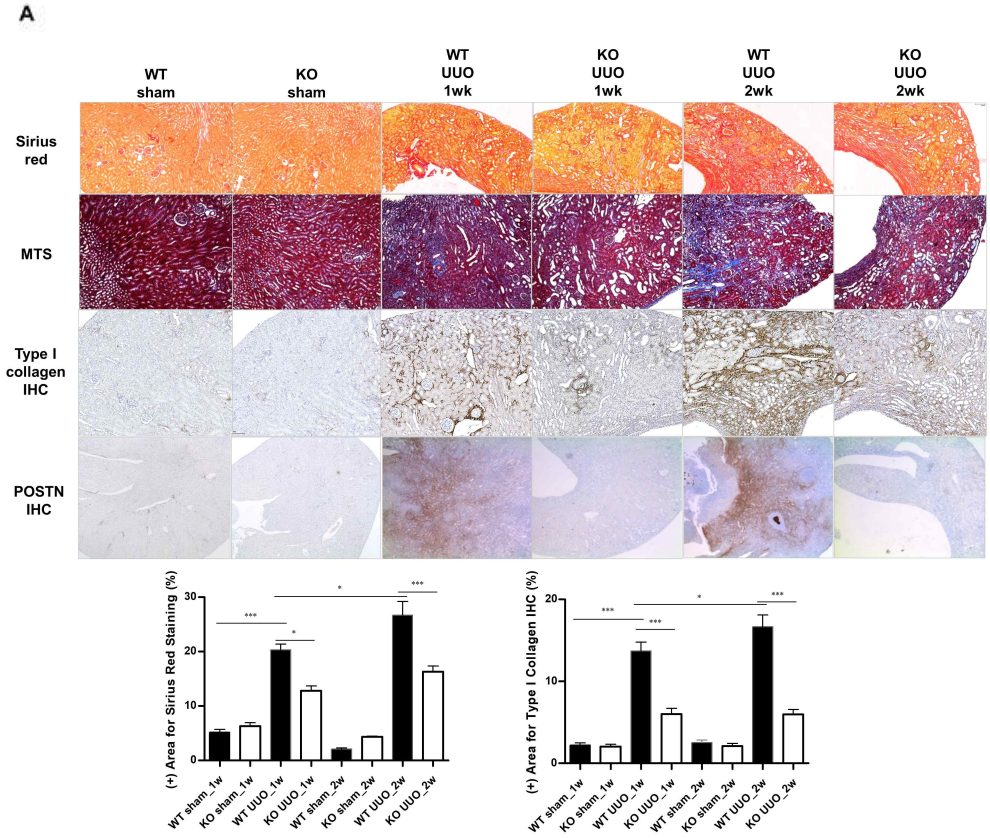
A
WT sham
KO sham
WT UUO 1wk
KO UUO 1wk
WT UUO 2wk
KO UUO 2wk
Sirius red
MTS
Type I collagen IHC
POSTN IHC
(+) Area for Sirius Red Staining (%)
(+) Area for Type I Collagen IHC (%)
WT sham_1w
KO sham_1w
WT UUO_1w
KO UUO_1w
WT sham_2w
KO sham_2w
WT UUO_2w
KO UUO_2w

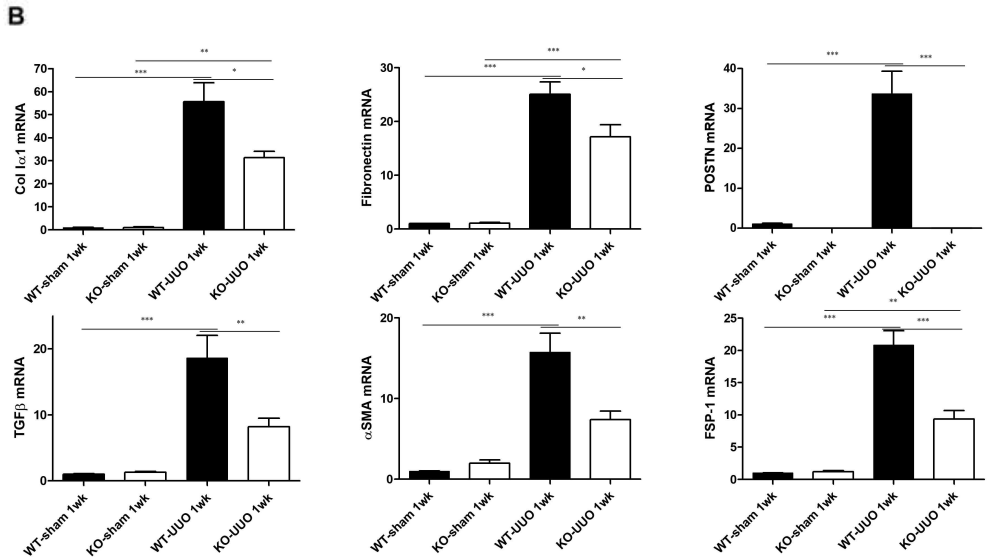
B
Col Iα1 mRNA
Fibronectin mRNA
POSTN mRNA
TGFβ mRNA
αSMA mRNA
FSP-1 mRNA
WT-sham 1wk
KO-sham 1wk
WT-UUO 1wk
KO-UUO 1wk

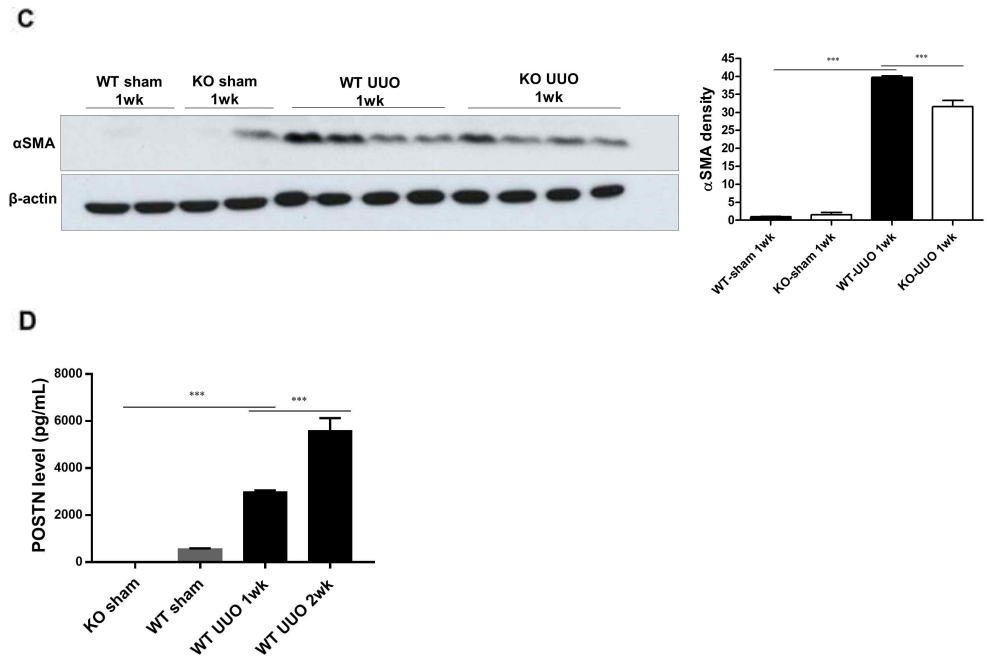

Figure 2. Fibrosis-related markers are highly induced by the UUO model and attenuated in the POSTN-KO mice.

A. Sirius Red staining, Masson's trichrome staining (MTS), type I collagen and periostin IHC sections in WT and POSTN-KO mice harvested 1 week and 2 weeks after the UUO operation are shown. The original magnification was ×100 for the Sirius Red staining, MTS, and type I collagen IHC and ×40 for the POSTN IHC. Five to seven fields were randomly selected from each kidney, and the red- or brown- stained area per total area, which reflects interstitial fibrosis, was quantified using a computer-based morphometric analysis software.

B. Quantification of POSTN and fibrosis-related mRNA shows that the increase in these indexes that was induced by the 1-week UUO model was attenuated in the POSTN-KO mice. C. Protein expression showed the

UUO-induced synthesis of αSMA.

D. Periostin ELISA confirmed that an increase in the synthesis of POSTN occurred in the UUO model.

Eight mice per strain were used in the sham group, fifteen mice were used in the WT UUO group, and sixteen mice were used in the KO-UUO group. Error bars represent the SEMs (*:$P < 0.05$, **:$P < 0.01$, ***:$P < 0.001$).

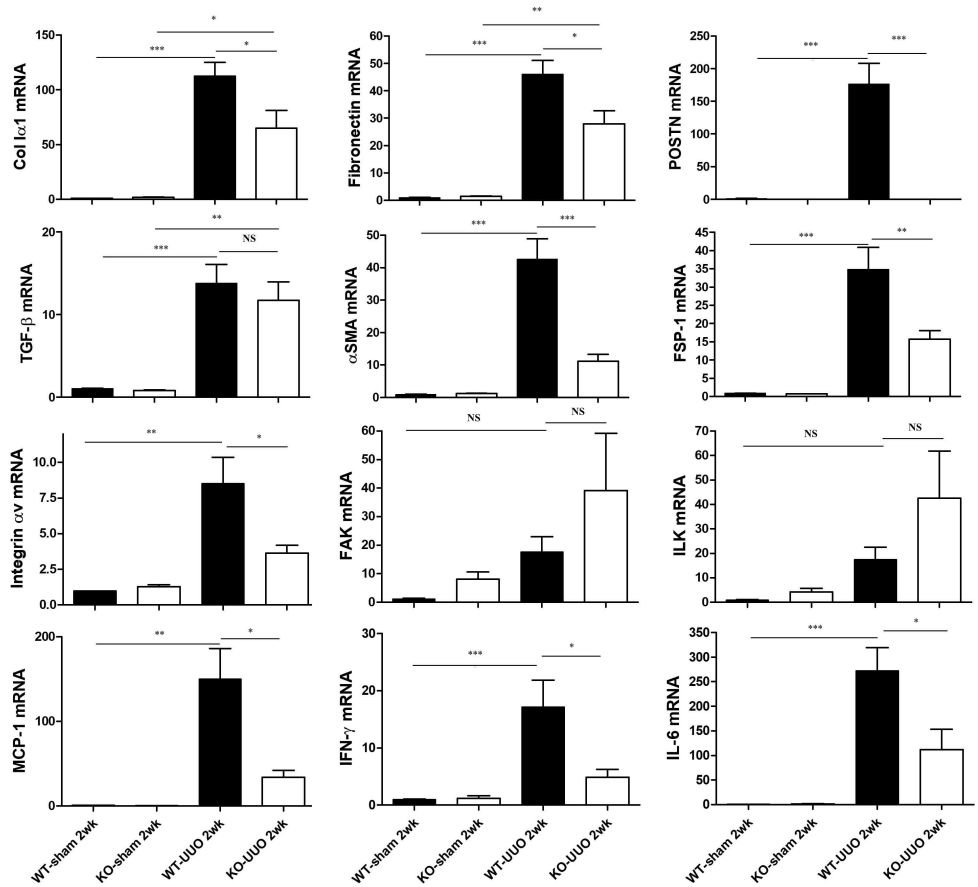

Figure 3. The 2-week UUO model showed a more prominent increase in fibrosis and inflammatory markers.

Two weeks after the UUO operation, the fibrosis- and inflammation-related mRNA expression showed a more prominent change than that observed in the 1-week model in the WT and POSTN-KO mice. Six and eight mice per strain were used in the WT and POSTN-KO sham groups, and fifteen mice were used in both UUO groups. Error bars represent the SEMs (*:$P < 0.05$, **:$P < 0.01$, ***:$P < 0.001$).

Expression of Inflammatory Markers in the UUO model in Wild-Type and Periostin-Deficient Mice

The UUO induces a strong inflammatory response and contributes to fibrosis. The qRT-PCR results showed that the mRNA expression levels of inflammatory cytokines, such as MCP-1, IFN-γ, and IL-6, were significantly increased in the WT mice and were decreased in the POSTN-KO mice (Figure 4A).

Macrophage, T-cell and neutrophil infiltration was evaluated using anti-F4/80, anti-CD3, and anti-neutrophil antibody immunofluorescence (IF), respectively in the 1-week UUO model. The immunostaining results showed a decreased infiltration of inflammatory cells in the POSTN-KO mice (Figure 4B). The decreased macrophage infiltration might be caused by the decreased expression of the proinflammatory cytokines.

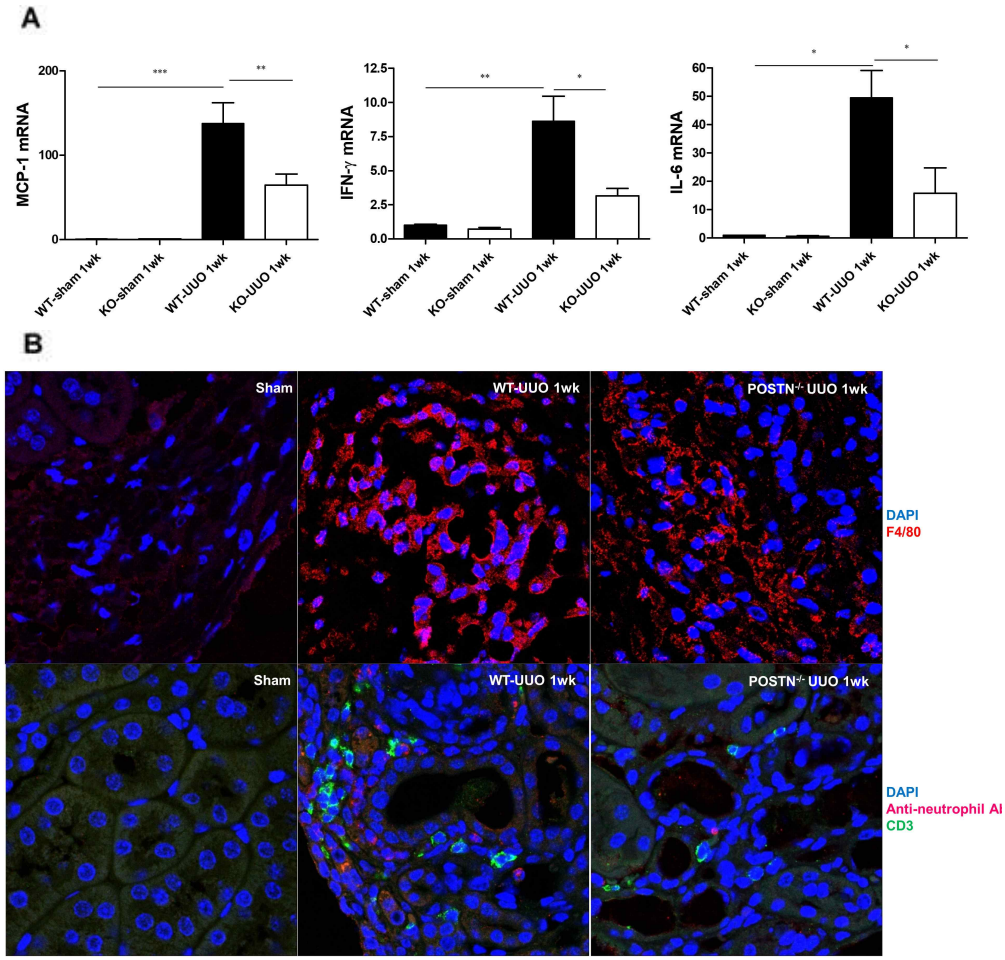

Figure 4. Inflammation markers are highly expressed in the UUO model and attenuated in the periostin-deficient mice.

A. Quantification of MCP-1, IFN-ɣ, and IL-6 mRNA shows that the increase in these indexes that was induced by the 1-week UUO model was attenuated in the POSTN-NO mice.

B. Macrophage, T-cell and neutrophil infiltration was evaluated by F4/80 (red-upper), CD3 (green), and anti-neutrophil (red-lower) antibody immunofluorescence and confocal microscopy (original magnification, × 600).

In the 1-week UUO model, a decrease in the infiltration of various inflammatory cells was observed in the POSTN-KO mice.

Eight mice per strain were used in the sham group, fifteen mice were used in the WT UUO group, and sixteen mice were used in the KO-UUO group. Error bars represent the SEMs (*:$P < 0.05$, **:$P < 0.01$, ***:$P < 0.001$).

Effects of Recombinant TGF-β and Recombinant Periostin in Primary Cultured Inner Medullary Collecting Duct Cells

We performed *in vitro* experiments using primary cultured IMCD cells to evaluate the cellular mechanisms that are associated with the fibrosis induction. The administration of rTGF-β increased periostin mRNA and FSP-1 protein expression in WT-IMCD cells in a dose-dependent manner (Figure 5A). The cell morphology was changed by the administered components, and rTGF-β plus rPOSTN resulted in the most prominent morphologic changes (Figure 5B). The combined administration of rTGF-β and rPOSTN synergistically stimulated periostin mRNA expression, and the mRNA expression was higher after the combined administration than after the individual administration of each component (Figure 5B). We induced fibrosis by rTGF-β, rPOSTN, or their combination and compared the responses in both WT and POSTN-KO mice cells. The results showed that αSMA mRNA expression was increased by the administration of rPOSTN, and a change in the cellular morphology was observed even though the intensity was lower than that observed with the administration of rTGF-β ($P < 0.001$; Figure 5B-C). The αSMA mRNA expression was attenuated in the POSTN-KO mice cells compared to that in the WT mice cells (Figure 5C). The αSMA protein also showed a similar tendency with a higher expression in the WT mice (Figure 5D). In summary, rTGF-β increased periostin expression by inducing the fibrotic environment, and rPOSTN individually and in combination with rTGF-β enhanced αSMA mRNA and protein expression.

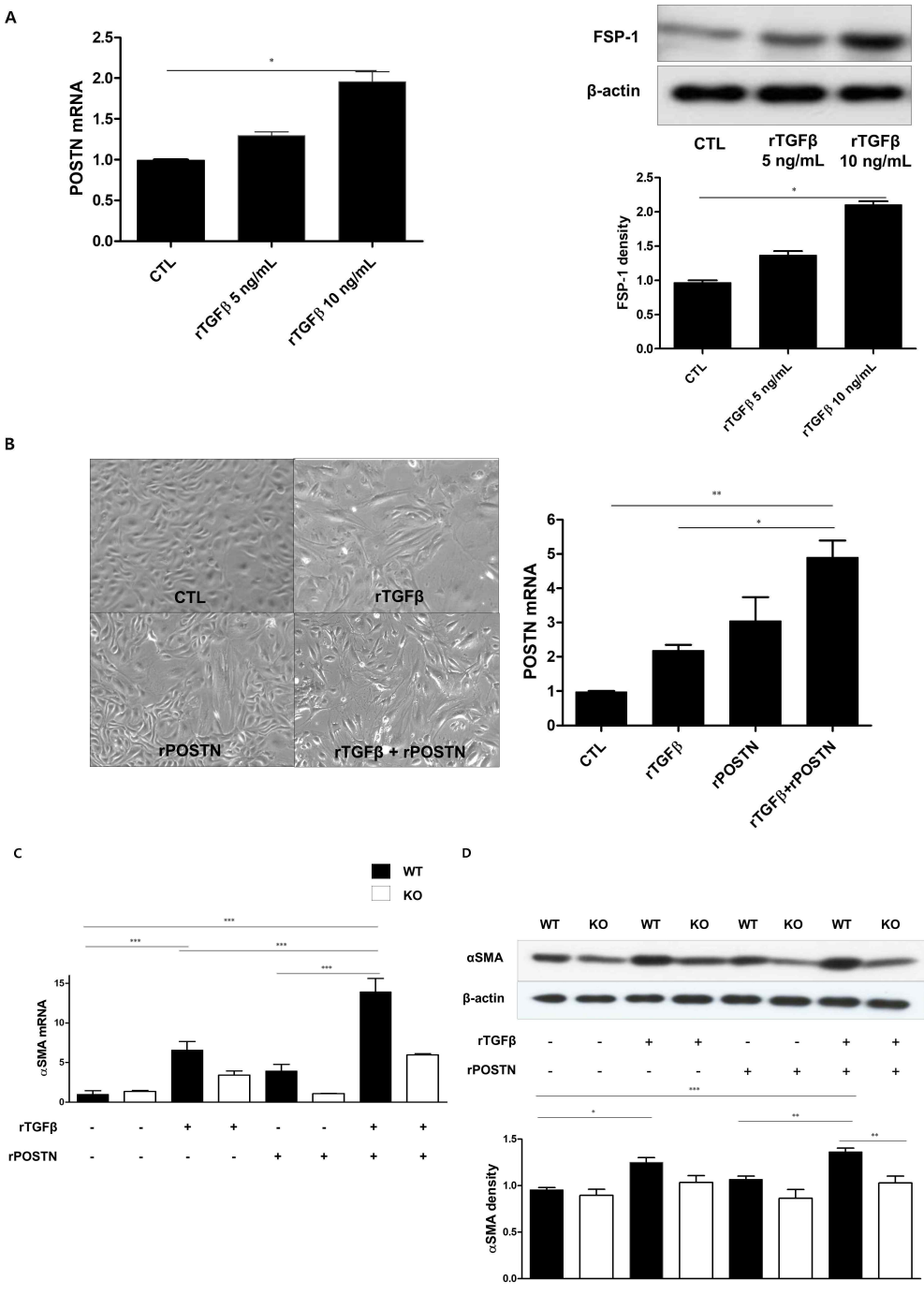
A
POSTN mRNA
2.5
2.0
1.5
1.0
0.5
0.0
*
CTL
rTGFβ 5 ng/mL
rTGFβ 10 ng/mL
FSP-1
β-actin
CTL
rTGFβ 5 ng/mL
rTGFβ 10 ng/mL
FSP-1 density
2.5
2.0
1.5
1.0
0.5
0.0
*
CTL
rTGFβ 5 ng/mL
rTGFβ 10 ng/mL
B
CTL
rTGFβ
rPOSTN
rTGFβ + rPOSTN
POSTN mRNA
6
5
4
3
2
1
0
**
*
CTL
rTGFβ
rPOSTN
rTGFβ+rPOSTN
C
WT
KO
αSMA mRNA
15
10
5
0
***
***
***
***
rTGFβ - - + + - - + +
rPOSTN - - - - + + + +
D
WT KO WT KO WT KO WT KO
αSMA
β-actin
rTGFβ - - + + - - + +
rPOSTN - - - - + + + +
αSMA density
1.5
1.0
0.5
0.0
***
*
**
**

Figure 5. The role of periostin in the *in vitro* fibrosis induction.

A. Recombinant TGF-β (rTGF-β) induced POSTN mRNA expression in primary cultured IMCD cells in a dose-dependent manner. The cells were treated with 5 or 10 ng rTGF-β for 72 hours, which resulted in a simultaneous increase in the FSP-1 protein expression.

B. Cell morphology was prominently changed by the administration of rTGF-β or recombinant POSTN (rPOSTN). Periostin mRNA expression was increased by the fibrosis induction with rTGF-β (5 ng/mL) or rPOSTN (1 μg/mL) in primary cultured IMCD cells. The combined administration of rTGF-β and rPOSTN showed a synergistic stimulation of periostin mRNA expression compared to that observed following the individual administration of rTGF-β or rPOSTN.

C. The αSMA mRNA expression that was induced by rTGF-β and rPOSTN was attenuated in the POSTN^{-}KOmicecells.

D. The protein expression of αSMA showed a similar increase and attenuation pattern in the WT and POSTN-KO mice cells.

Error bars represent the SEMs (*:$P < 0.05$, **:$P < 0.01$, ***:$P < 0.001$).

Expression of Integrin and the Effect of Integrin Blockade

Periostin is known as a ligand of integrin, and our experiment showed an increased expression of integrin αv, β3, and β5 mRNA in the UUO model. The integrin expression pattern was similar to that observed in other fibrosis-related mRNA (Figure 6A). The *in vitro* administration of rTGF-β or rPOSTN to primary cultured IMCD cells from WT mice increased the expression of integrin mRNA. However, the elevated patterns in the groups treated with rPOSTN alone and those treated with rTGF-β + rPOSTN were different according to the integrin subtypes. A synergistic effect of rTGF-β + rPOSTN was not observed in any of the components except for integrin β3 (Figure 6B). Based on these results, integrin was thought to participate in renal fibrosis, and the integrin-blocking tetrapeptide Arg-Gly-Asp-Ser (RGDS) peptide was administered to block the POSTN-binding pathway. The treatment with RGDS decreased the Col Iα1, fibronectin, and αSMA mRNA expression levels in both the WT and KO mice cells. The degree of fibrosis-related mRNA expression and its reduction by RGDS were more prominent in the WT mice cells than in the KO mice cells, which has also been shown in other results. The elevated αSMA mRNA expression caused by rPOSTN was significantly decreased by the combined RGDS administration to the WT mice cells ($P < 0.01$; Figure 6C).

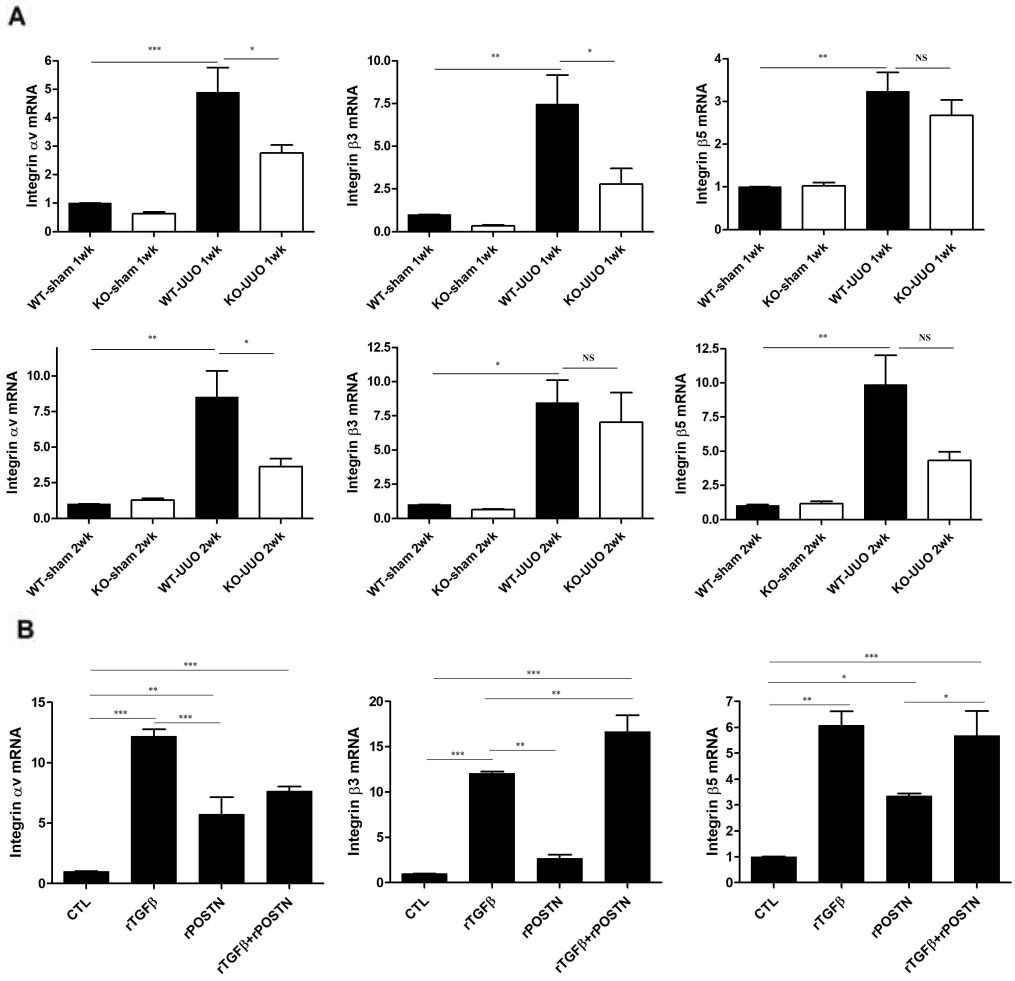
A
Integrin αv mRNA
Integrin β3 mRNA
Integrin β5 mRNA
WT-sham 1wk
KO-sham 1wk
WT-UUO 1wk
KO-UUO 1wk
WT-sham 2wk
KO-sham 2wk
WT-UUO 2wk
KO-UUO 2wk
NS
B
CTL
rTGFβ
rPOSTN
rTGFβ+rPOSTN

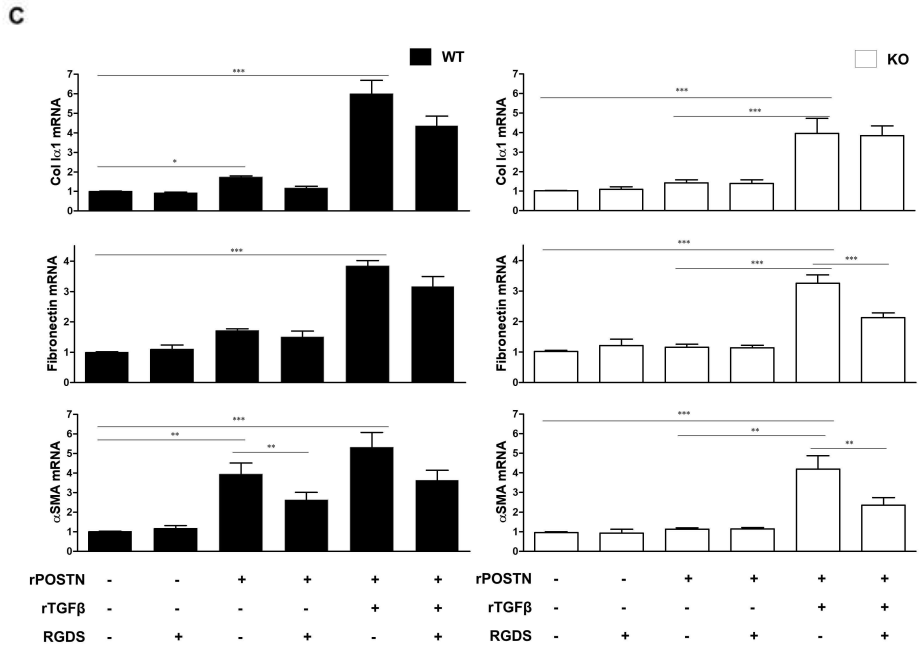

Figure 6. Integrin association with the UUO-induced fibrosis and integrin blockade fibrosis induction.

A. The UUO-induced increase of integrin αv, β3, and β5 mRNA expression was blunted in the POSTN-KO mice.

B. The elevated patterns of integrin mRNA expression in the groups treated with rPOSTN alone (1 μg/mL) and rTGF-β (5 ng/mL) + rPOSTN (1 μg/mL) were different across the integrin subtypes. There was no synergistic effect of rTGF-β + rPOSTN compared to the effect of each of the components individually except for integrin β3.

C. Treatment with RGDS decreased Col Iα1, fibronectin, and αSMA mRNA expression levels in both the WT and POSTN-KO mice cells. The degree of fibrosis-related mRNA expression was higher in the WT mice cells than in the POSTN-KO mice cells.

Effect of Periostin Blockade in In Vivo and In Vitro Fibrosis Models

To determine whether the beneficial effects of the periostin inhibition in attenuating tissue fibrosis were also producible by an anti-POSTN antibody, we evaluated the severity of fibrosis in kidneys from WT mice that were treated with an aPOSTNab or an isotype IgG on 4 separate days following the UUO (days 0, 2, 4, and 6). Based on images of the kidney sections that were stained with Sirius Red and type I collagen IHC, the kidneys from the WT UUO and UUO + isotype IgG groups had increased fibrosis compared to those in the WT sham group. The treatment with aPOSTNab significantly attenuated the fibrosis in the UUO kidneys. In the morphometric analysis, the collagen positive area increased in the WT mice ($P < 0.001$), and the mice that were treated with aPOSTNab showed a significant decrease in fibrous tissue ($P < 0.001$, Figure 7A).

The administration of aPOSTNab in the UUO model significantly reduced the Col Iα1, αSMA and MCP-1 mRNA expression compared to that observed in the UUO or UUO + isotype IgG groups (Figure 7B). Fibronectin, ILK and FAK mRNA expression showed a tendency that was similar to that observed in the other fibrosis-related proteins (Figure 7B). The fibrosis-related protein also showed a decrease in expression after the aPOSTNab injection (Figure 7C). The anti-F4/80 IF revealed a decrease in macrophage infiltration in the UUO + aPOSTNab groups compared with that in the UUO group (39.2 ± 6.7% vs. 60.0 ± 11.3%, respectively), which was correlated with the MCP-1 mRNA expression (Figure 7D). Apoptotic markers, such as p53, and the TUNEL assay were also evaluated, and a

similar decrease in the aPOSTNab treatment group was observed ($P < 0.01$ for the TUNEL, $P < 0.001$ for p53 mRNA). Anti-apoptotic Bcl-2 showed the opposite tendency; and its lowest expression occurred in the UUO group ($P < 0.05$) and a significant increase occurred in the aPOSTNab group ($P < 0.01$, Figure 7E). The *in vitro* study showed similar results in that the administration of rPOSTN more prominently increased αSMA, Col Iα1, and fibronectin mRNA expression in the WT mice cells than in the POSTN-KO mice cells. The administration of aPOSTNab attenuated the rPOSTN-induced fibrosis in the WT mice cells (Figure 7F). Taken together, the periostin blockade effectively attenuated fibrosis by decreasing inflammatory cytokines and apoptotic signals.

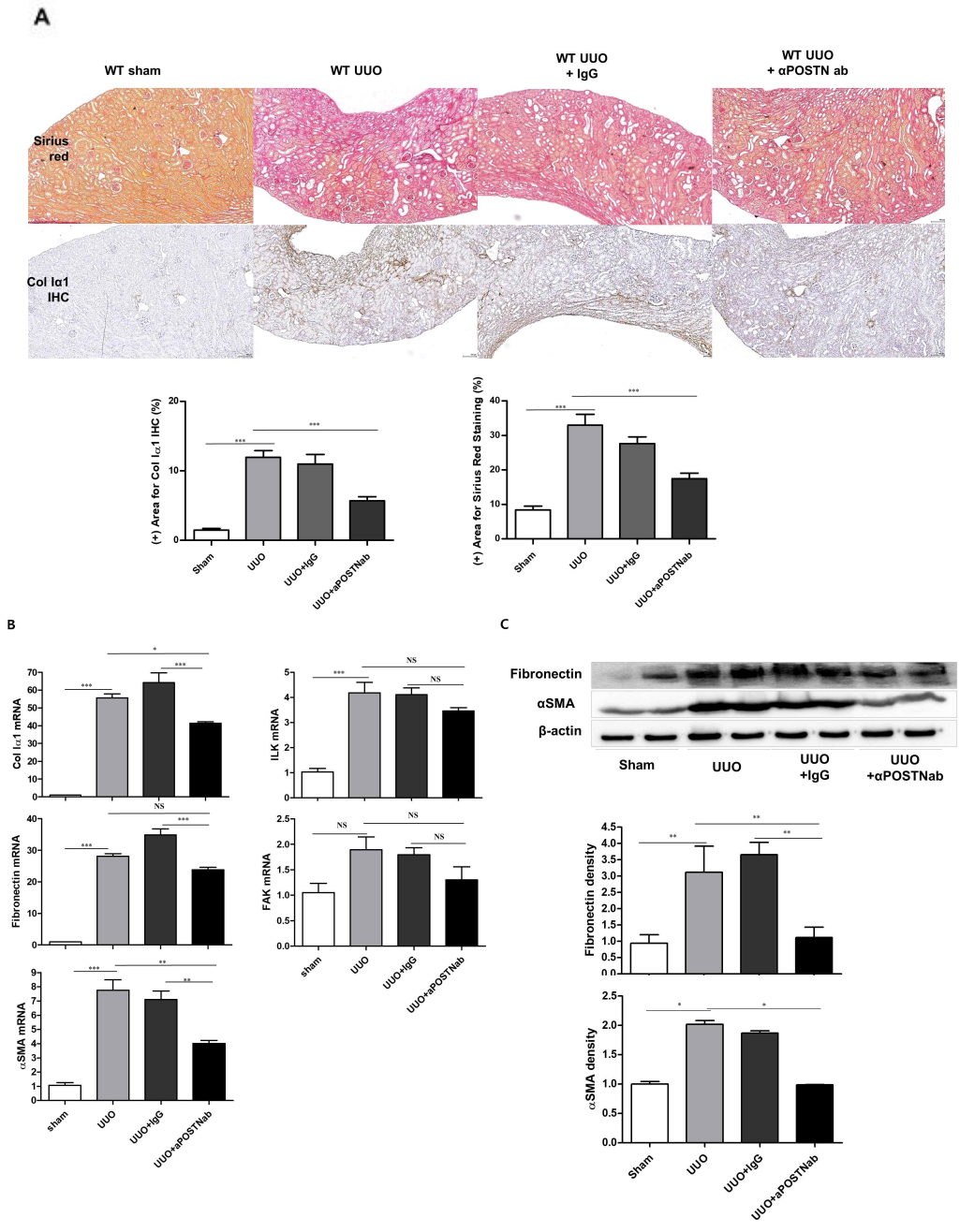
A
WT sham
WT UUO
WT UUO + IgG
WT UUO + αPOSTN ab
Sirius red
Col Iα1 IHC
(+) Area for Col Iα1 IHC (%)
(+) Area for Sirius Red Staining (%)
Sham
UUO
UUO+IgG
UUO+αPOSTNab
B
Col Iα1 mRNA
ILK mRNA
Fibronectin mRNA
FAK mRNA
αSMA mRNA
sham
UUO
UUO+IgG
UUO+αPOSTNab
C
Fibronectin
αSMA
β-actin
Sham
UUO
UUO +IgG
UUO +αPOSTNab
Fibronectin density
αSMA density

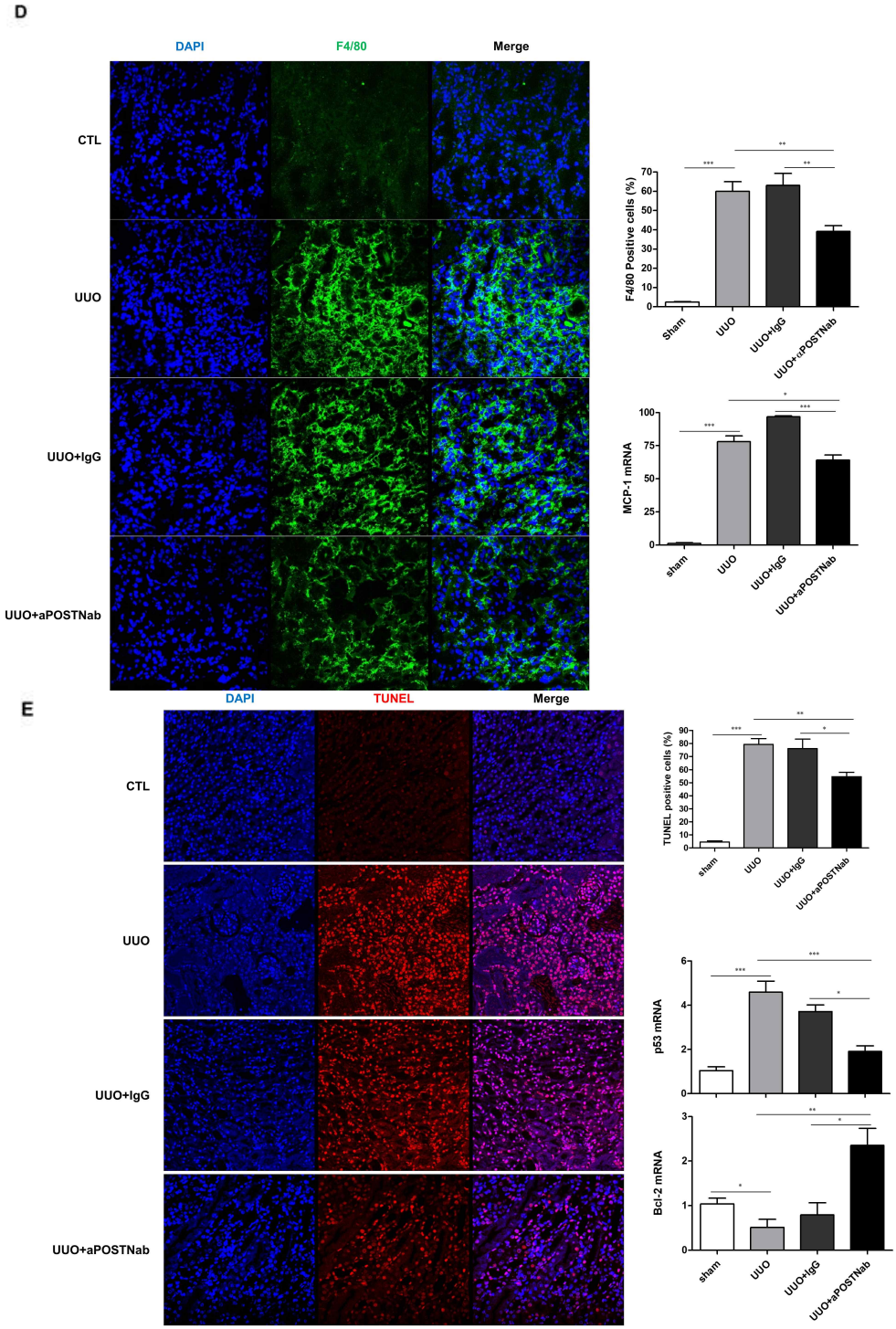
D
DAPI
F4/80
Merge
CTL
UUO
UUO+IgG
UUO+aPOSTNab
F4/80 Positive cells (%)
Sham
UUO
UUO+IgG
UUO+αPOSTNab
MCP-1 mRNA
sham
UUO
UUO+IgG
UUO+aPOSTNab
E
DAPI
TUNEL
Merge
CTL
UUO
UUO+IgG
UUO+aPOSTNab
TUNEL positive cells (%)
sham
UUO
UUO+IgG
UUO+aPOSTNab
p53 mRNA
Bcl-2 mRNA
sham
UUO
UUO+IgG
UUO+aPOSTNab

Figure 7. Periostin blockade by an anti-POSTN polyclonal antibody (aPOSTNab) attenuated fibrosis and inflammation.

A. Sirius Red staining and type I collagen IHC showed that the kidneys from the WT UUO and UUO + isotype IgG groups had increased fibrosis compared to that in the WT sham group (UUO 1-week model). Treatment with aPOSTNab significantly attenuated the fibrosis in the UUO kidney.

B. Administration of aPOSTNab in the UUO model significantly reduced Col Iα1, αSMA and MCP-1 mRNA expression compared to that in the UUO or UUO + isotype IgG groups. Fibronectin, integrin-linked kinase (ILK) and focal adhesion kinase (FAK) mRNA expression showed a tendency that similar to that observed in the other proteins.

C. An increase in type I collagen, fibronectin and αSMA protein expression occurred after UUO was attenuated with aPOSTNab.

D. Macrophage infiltration was evaluated by F4/80 (green) immunofluorescence and confocal microscopy (original magnification, × 200) in the 1-week UUO model, and the results showed a decreased infiltration of macrophages after the administration of aPOSTNab. In the UUO + aPOSTNab group, MCP-1 mRNA expression was decreased.

E. Apoptotic markers, such as p53 mRNA expression, and the TUNEL assay showed a similarly decreased pattern in the aPOSTNab treatment group. Anti-apoptotic Bcl-2 mRNA showed an inversed pattern with a decreased expression in the UUO group and a marked expression in the UUO + aPOSTNab group.

F. Treatment with aPOSTNab decreased the Col Iα1, fibronectin, and αSMA mRNA expression levels in both the WT and POSTN-KO mice cells.

Baseline Characteristics by Urine and Plasma POSTN Grouping

The study flow chart is shown in Figure 8. The distribution of plasma periostin, the uPOSTN/Cr levels of healthy subjects and of IgAN patients, and the natural logarithm transformed (ln) uPOSTN/Cr level of these patients are shown in Figure 9A, 9B and 9C, respectively. Table 1 summarizes baseline characteristics of the study populations by uPOSTN/Cr level; 148 patients who had undetected uPOSTN level by ELISA were categorized into group 1. Remaining patients with uPOSTN levels measured by ELISA were divided into group 2 and group 3 by the median value (median uPOSTN/Cr, 628.1 pg/mgCr). Systolic and diastolic blood pressures were higher and eGFR at the time of renal biopsy was lower in group 3. Pathologic classifications were compared between groups, and patients with advanced grades or classes were distributed significantly more in group 3 (Table 1). Total follow-up duration was 27.1 months, and that of groups 1, 2, and 3 was 20.9, 29.1, and 32.9 months, respectively ($P < 0.001$).

The quartile groups by plasma periostin level did not show significant differences in most of the parameters between groups (Table 2). In correlation analysis, uPOSTN/Cr was weakly associated with plasma POSTN ($r = 0.232$; $P = 0.007$; Figure 9D). Urinary POSTN/Cr showed negative correlation with eGFR at the time of renal biopsy ($r = 0.245$; $P = 0.001$; Figure 9E) and showed no significant relationship with uPCr (Figure 9F).

Figure 7G-7I shows the ln-uPOSTN/Cr levels in significant pathologic findings. The patients with IF/TA ($P = 0.003$; Figure 9G),

interstitial inflammation (P = 0.046; Figure 9H), and hyaline arteriolosclerosis (P = 0.013; Figure 9I) showed higher ln-uPOSTN/Cr levels than the others.

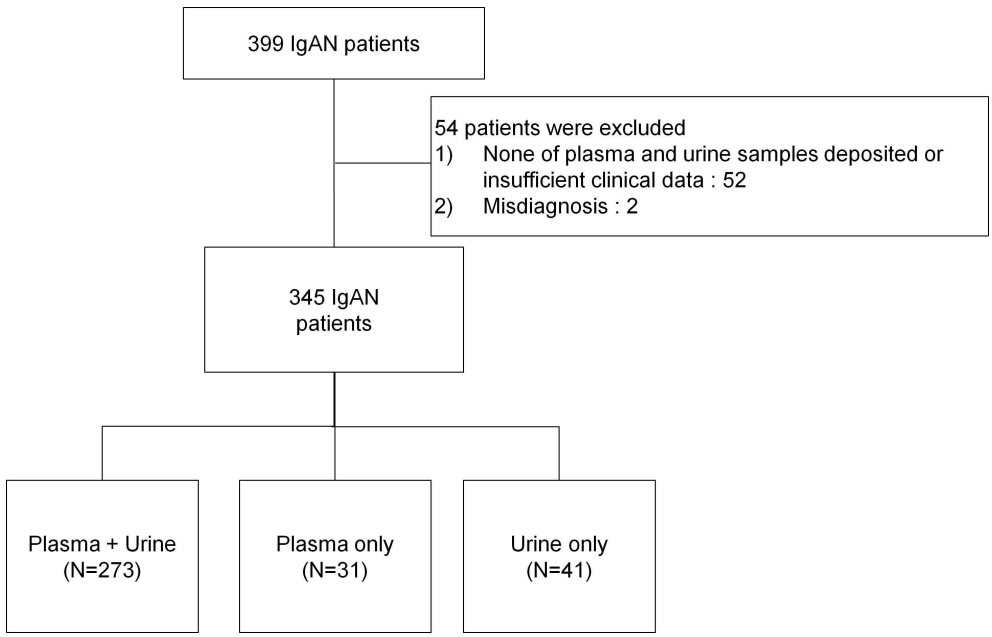

Figure 8. Flow chart of IgA nephropathy patients in the cohort.

We reviewed the medical records of 399 individuals and collected data of 345 patients.

Table 1. Baseline characteristics of the IgA nephropathy patients by uPOSTN/Cr

	Urine POSTN/Cr				*P* value
	Group 1 (n=148)	Group 2 (n=83)	Group 3 (n=83)	Total (N=314)	
Urine POSTN/Cr (pg/mgCr)*	0	208.6 (8.6-614.5)	1833.1 (641.7-10535.2)	46.6 (0-10535.2)	<0.001
Plasma POSTN (ng/mL)*	68.6 (18.7-2711.0)	58.2 (13.8-1927.4)	102.6 (7.4-2374.7)	84.1 (7.4-2711.0)	0.178
Age (year)	38.3±15.2	40.5±15.5	43.1±14.2	40.2±15.1	0.066
Male Sex (%)	48.6	60.2	38.6	49.0	0.020
BMI (kg/m^2)	23.0±3.5	23.5±3.1	22.5±3.3	23.0±3.3	0.417
Systolic BP (mmHg)	122.6±17.6	119.5±17.8	127.0±20.4	122.9±18.5	0.039[c]
Diastolic BP (mmHg)	77.0±13.4	76.0±11.4	81.5±12.9	77.9±12.9	0.013[bc]
Comorbidity DM (%)	3.5	4.9	7.4	4.9	0.423
HBV infection (%)	3.2	4.0	5.2	4.0	0.773
Serum IgA level (mg/dL)	305.5 ±105.1	311.6 ±102.0	317.2 ±105.5	310.4 ±104.1	0.754
Serum creatinine (mg/dL)	1.24±1.22	1.38±1.56	1.53±1.16	1.35±1.31	0.255
IDMS-MDRD eGFR (mL/min/1.73m^2)	80.6±34.5	74.1±31.2	58.7±27.3	73.1±33.0	<0.001[bc]
Serum albumin (g/dL)	3.8±0.6	4.0±0.4	3.7±0.5	3.8±0.5	0.004[cd]
Cholesterol (mg/dL)	191.7±43.0	182.2±34.2	186.3±34.9	187.8±38.9	0.199
Uric acid (mg/dL)	5.9±1.8	6.0±1.5	6.5±1.8	6.1±1.7	0.025[b]
hs-CRP (mg/dL)	0.32±0.60	0.21±0.53	0.35±1.08	0.29±0.72	0.509
Spot urine Protein/Cr (g/g Cr)	1.96±2.30	1.56±2.61	1.78±1.93	1.81±2.30	0.449
Patients with spot urine protein/Cr ≥ 1 g/gCr (%)					

Pathologic Classification (%)	WHO Class I	17.8	8.1	8.6	11.9	<0.001
	Class II	49.3	54.8	15.5	40.9	
	Class III	24.7	21.0	22.4	22.8	
	Class IV	4.1	9.7	34.5	15.0	
	Class V	4.1	6.5	19.0	9.3	
	Lee SMK Grade I	2.3	2.6	4.5	2.9	0.001
	Grade II	34.6	21.8	28.8	29.6	
	Grade III	44.4	60.3	27.3	44.8	
	Grade IV	14.3	14.1	25.8	17.0	
	Grade V	4.6	1.3	13.6	5.8	
	Haas Class I	2.3	2.6	6.1	3.2	0.048
	Class II	5.3	1.3	6.1	4.3	
	Class III	28.6	23.1	22.7	25.6	
	Class IV	51.9	60.3	36.4	50.5	
	Class V	12.1	12.8	28.8	16.2	
IFTA	Severity (score)[a]	1.00±0.61	1.10±0.59	1.29±0.57	1.10±0.61	0.004[c]
	Moderate to severe (%)	17.1	23.1	31.5	22.3	0.03
Interstitial inflammation	Severity (score)[a]	0.89±0.63	0.95±0.50	1.16±0.62	0.98±0.60	0.007[c]
	Moderate to severe (%)	13.5	10.1	28.0	16.2	0.008
Mesangial hypercellularity (%)		97.2	98.8	91.2	96.1	0.03
Vessel Fibrointimal thickening (%)		43.4	40.7	55.7	45.9	0.118
Hyaline arteriolo-sclerosis (%)		12.4	8.6	27.8	15.4	0.001
Segmental sclerosis		5.6±7.6	6.1±7.5	8.5±10.2	6.5±8.4	0.048[c]

(mean of %)					
Global sclerosis (mean of %)	19.3±22.3	19.5±20.9	30.5±24.3	22.2±22.9	0.001[cd]
Segmental+global sclerosis (mean of %)	24.9±24.8	25.7±24.7	38.9±27.1	28.7±26.0	<0.001[cd]
Crescent (mean of %)	1.3±3.8	0.7±2.5	2.3±6.6	1.4±4.5	0.060

Note: Values for categorical variables are given as percentage; values for continuous variables, as mean ± standard deviation.

Abbreviations: POSTN, periostin; Cr, creatinine; BMI, body mass index; BP, blood pressure; DM, diabetes mellitus; HBV, hepatitis B virus; IDMS, isotope dilution mass spectrometry traceable; eGFR, estimated glomerular filtration rate; CRP, C-reactive protein; IFTA, interstitial fibrosis/tubular atrophy; ACEi, angiotensin converting enzyme inhibitor; ARB, angiotensin II receptor blocker.

[*] Data were expressed as median (min-max).

[a] Mean value of severity was calculated by none (0), mild (1, ≤ 25%), moderate (2, 26-50%), severe (3, > 50%).

[b] $P < 0.05$ at post-hoc analysis between group 1 and 3

[c] $P < 0.05$ at post-hoc analysis between group 2 and 3

[d] $P < 0.05$ at post-hoc analysis between group 1 and 2.

Table 2. Baseline characteristics of the study subjects by plasma POSTN

		Plasma POSTN					
		Group 1 (n=76)	Group 2 (n=76)	Group 3 (n=76)	Group 4 (n=76)	Total (N=304)	*P* value
Plasma POSTN (ng/mL)*		244.3 (104.5 -364.4)	497.5 (378.0 -599.0)	730.0 (608.2 -844.8)	1216.1 (860.1 -2711.0)	84.1 (7.4 -2711.0)	<0.001[b]
Age (year)		40.2±12.7	40.1±15.5	35.0±15.1	40.8±15.2	39.0±14.8	0.051
Male Sex (%)		53.9	43.4	50.0	51.3	49.7	0.609
BMI (kg/m^2)		23.7±3.0	23.1±3.8	22.3±2.6	23.4±2.7	22.9±2.9	0.193
Systolic BP (mmHg)		120.1 ±20.5	121.4 ±15.1	124.1 ±2.2	125.2 ±15.3	122.7 ±18.0	0.287
Diastolic BP (mmHg)		77.2±13.2	75.8±11.6	76.9±13.9	80.4±11.2	77.6±12.6	0.137
Comorbidity	DM (%)	4.0	2.8	5.3	5.3	4.4	0.856
	HBV infection (%)	3.2	1.8	1.4	7.9	3.7	0.136
Serum IgA level (mg/dL)		311.6 ±113.7	295.0 ±95.5	300.6 ±91.0	337.2 ±117.5	311.6 ±105.6	0.102
Serum creatinine (mg/dL)		1.59±2.20	1.16±0.59	1.47±1.21	1.25±0.92	1.37±1.37	0.204
IDMS_eGFR (mL/min/1.73m^2)		76.1±35.9	74.7±31.1	74.9±38.2	70.6±27.3	74.1±33.3	0.751
Serum albumin (g/dL)		3.9±0.5	3.9±0.5	3.8±0.5	3.8±0.5	3.8±0.5	0.568
Cholesterol (mg/dL)		183.7 ±32.2	191.9 ±39.0	185.1 ±36.5	187.0 ±46.7	186.9 ±38.9	0.594
Uric acid (mg/dL)		6.2±1.9	5.9±1.8	6.0±1.7	6.3±1.6	6.1±1.8	0.496
hs-CRP (mg/dL)		0.24±0.45	0.21±0.54	0.23±0.54	0.44±1.09	0.28±0.69	0.266
Spot urine Prot/Cr (g/gCr)		1.26±1.20	1.69±2.44	2.08±2.89	1.86±2.12	1.72±2.26	0.153

Pathologic Classification (%)	WHO Class I	15.2	11.1	8.3	11.1	10.9	0.679
	Class II	42.4	44.4	41.7	41.3	42.2	
	Class III	21.2	13.9	26.7	25.4	22.9	
	Class IV	6.1	25.0	15.0	15.9	15.6	
	Class V	15.2	5.6	8.3	6.3	8.3	
	LeeSMK Grade I	1.4	6.0	0	3.1	2.5	0.214
	Grade II	34.2	28.4	25.4	25.0	28.4	
	Grade III	37.0	46.3	50.7	51.6	46.2	
	Grade IV	23.3	16.4	14.1	15.6	17.5	
	Grade V	4.1	3.0	9.9	4.7	5.5	
	Haas Class I	1.4	9.0	0	1.6	2.9	0.104
	Class II	8.2	4.5	0	6.3	4.7	
	Class III	27.4	22.4	23.6	22.2	24.0	
	Class IV	45.2	49.3	59.7	57.1	52.7	
	Class V	17.8	14.9	16.7	12.7	15.6	
IFTA	Severity (score)[a]	1.16±0.50	1.03±0.62	1.07±0.63	1.01±0.69	1.07±0.61	0.439
	Moderate to severe (%)	21.9	20.5	20.6	21.3	21.1	0.313
Interstitial inflammation	Severity (score)[a]	1.04±0.58	0.95±0.62	0.94±0.64	0.91±0.67	0.96±0.63	0.598
	Moderate to severe (%)	18.7	13.6	17.4	17.6	16.7	0.533
Mesangial hypercellularity	(%)	96.1	96.1	97.3	93.4	95.7	0.684
Vessel	Fibro -intimal thickening	44.7	47.4	45.3	42.1	44.9	0.934

(%)						
Hyaline arteriolo-sclerosis (%)	18.4	9.2	13.3	19.7	15.2	0.246
Segmental sclerosis (mean of %)	6.3±7.6	6.1±8.5	7.1±8.5	6.6±7.5	6.6±8.0	0.712
Global sclerosis (mean of %)	24.1±24.5	20.0±20.2	23.4±25.1	21.7±22.6	22.3±23.1	0.778
Segmental+global sclerosis (mean of %)	30.5±28.0	26.1±23.9	30.5±28.5	28.2±23.3	28.8±26.0	0.684
Crescent (mean of %)	0.8±2.9	0.9±2.7	1.7±4.9	1.8±6.1	1.3±4.4	0.299

Note: Values for categorical variables are given as percentage; values for continuous variables, as mean ± standard deviation.

* Data were expressed as median (min-max).

Abbreviations: POSTN, periostin; Cr, creatinine; BMI, body mass index; BP, blood pressure; DM, diabetes mellitus; HBV, hepatitis B virus; IDMS, isotope dilution mass spectrometry traceable; eGFR, estimated glomerular filtration rate; CRP, C-reactive protein; IFTA, interstitial fibrosis and tubular atrophy; ACEi, angiotensin converting enzyme inhibitor; ARB, angiotensin II receptor blocker.

[a] Mean value of severity was calculated by none (0), mild (1, $\leq$ 25%), moderate (2, 26-50%), severe (3, > 50%).

[b] $P < 0.05$ between the all groups

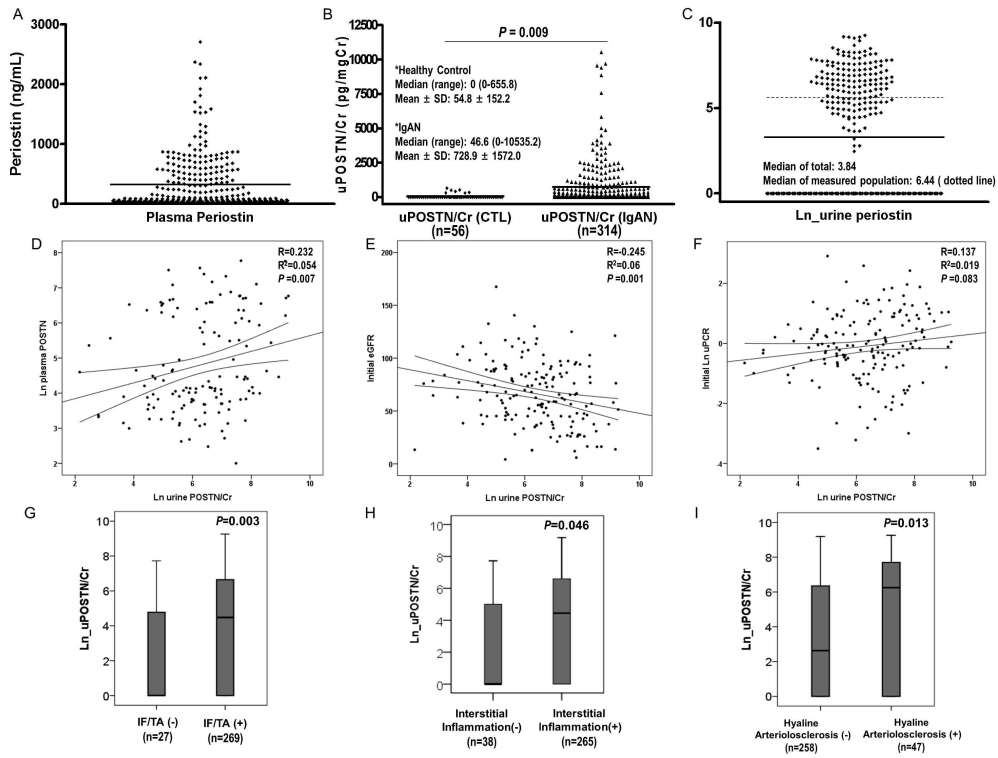

Figure 9. Relationships between uPOSTN/Cr and clinical parameters.

Distribution of (A) plasma periostin (ng/mL) and (B) uPOSTN/Cr in healthy control (CTL) compared with patients with IgA nephropathy, and as well as (C) natural log transformed (ln-) levels of uPOSTN/Cr. (D) Correlation between uPOSTN/Cr and plasma POSTN (r = 0.232, P = 0.007). (E) Correlation between uPOSTN/Cr and initial eGFR (r = -0.245, P = 0.001). (F) Correlation between uPOSTN/Cr and initial uPCR (r = 0.137, P = 0.083). Ln-uPOSTN/Cr level (G) with or without interstitial fibrosis/tubular atrophy (IF/TA) (P = 0.003), (H) by interstitial inflammation (P = 0.046), and (I) by hyaline arteriolosclerosis (P = 0.013)

Renal Outcomes

ESRD developed in 28 patients during the mean 27.1 months of follow-up. We evaluated the renal outcomes between group 1 + 2 and group 3 because baseline characteristics were significantly different particularly in group 3. All the renal outcomes with ESRD (P = 0.003), ESRD and/or eGFR decrease > 30% (P = 0.033), and ESRD and/or eGFR decrease > 50% (P = 0.046) occurred significantly more in group 3 as per Kaplan-Meyer survival analyses (Figure 10A-10C).

The patients with ESRD (P < 0.001), eGFR decrease >30% (P = 0.002), and eGFR decrease > 50% (P = 0.046) showed higher ln-uPOSTN/Cr levels than patients without these renal outcomes (Figure 10D-10F). We conducted multivariate analysis for the occurrence of ESRD. When we adjusted for age, sex, uPCr, and serum creatinine at the time of renal biopsy, and uPOSTN-based grouping, we found that uPCr (P < 0.001), serum creatinine (P < 0.001), and uPOSTN group 3 (hazards ratio, 2.839 vs. group 1 + 2; confidence interval, 1.013-7.957; P = 0.047) independently associated with ESRD in IgAN patients (Table 3).

We compared annual eGFR decrease (ΔeGFR/year) only in patients followed up for more than 1 year. The patients in group 3 (high uPOSTN/Cr), those with initial eGFR $\geq$60 ml/min/1.73 m^2(P = 0.043) and < 60 ml/min/1.73 m^2(P = 0.025), showed a rapid decline in renal function (Figure 11).

The ROC analysis of urine periostin (pg/mgCr) in predicting ESRD in IgAN is illustrated in Figure 12. Urinary POSTN/Cr > 1354.5 pg/mgCr demonstrates a 74.1% specificity and 73.7% sensitivity for predicting ESRD

occurrence. The performance of uPOSTN/Cr at the time of renal biopsy in predicting ESRD is also demonstrated in Figure 12. There was only a weak effect of incremental increases in uPOSTN/Cr level on serum creatinine and uPCr levels.

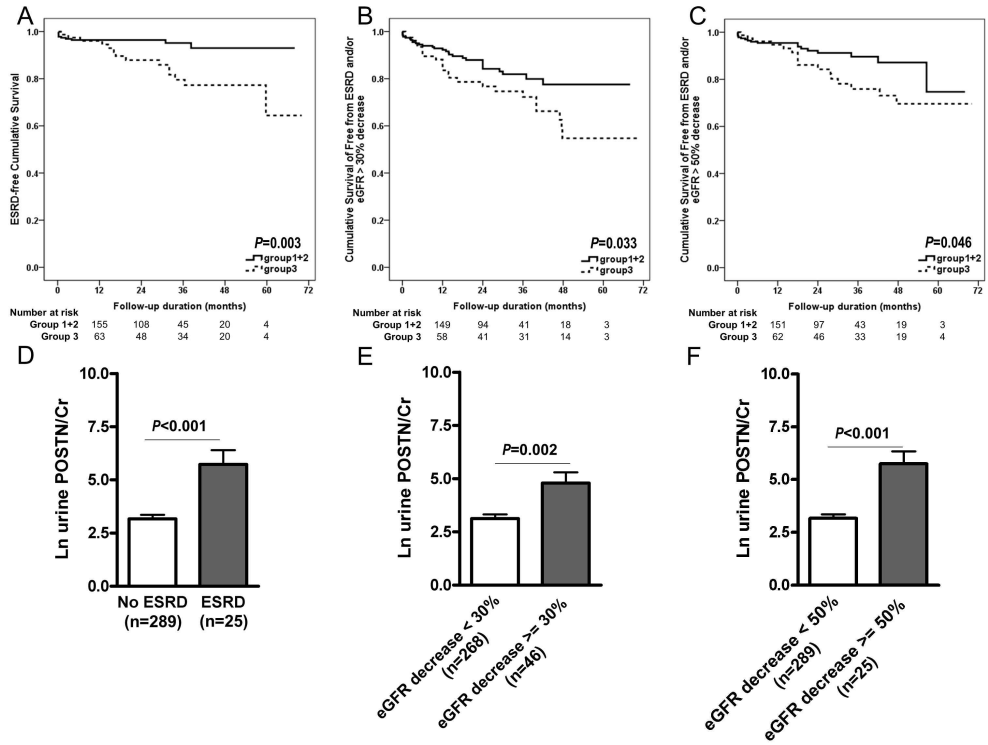

Figure 10. Renal outcome evaluation.

Kaplan-Meier curve (A) for the occurrence of ESRD (log-rank P = 0.003), (B) for ESRD and/or eGFR decrease > 30% (log-rank P = 0.033), and (C) for the ESRD and/or eGFR decrease > 50% (log-rank P = 0.046) showed significant differences between group 1 + 2 and group 3. (D) The patients with ESRD (P < 0.001), (E) eGFR decrease > 30% (P = 0.002), and (F) eGFR decrease > 50% (P = 0.046) showed higher ln-uPOSTN/Cr levels than patients without renal outcome.

Table 3. Multivariate analysis for the occurrence of ESRD

	Univariate		Multivariate	
	HR (95% CI)	***P* value**	**HR (95% CI)**	***P* value**
Age (per 1-year-old increase)	1.011 (0.985-1.038)	0.422	0.960 (0.926-0.995)	**0.026**
Male	1.575 (0.722-3.435)	0.254	0.895 (0.337-2.379)	0.824
Urine POSTN group 1+2	Reference		Reference	
group 3	2.997 (1.301-6.901)	**0.010**	2.839 (1.013-7.957)	**0.047**
Laboratory findings at the time of kidney biopsy				
uPCr (per 1g/gCr increase)	1.233 (1.148-1.324)	**<0.001**	1.406 (1.225-1.614)	**<0.001**
Serum Cr (per 1 mg/dL increase)	2.353 (1.943-2.851)	**<0.001**	3.270 (2.288-4.673)	**<0.001**

Abbreviations: POSTN, periostin; uPCr, urine protein/creatinine ratio; Cr, creatinine; HR, hazard ratio; CI, confidence interval.

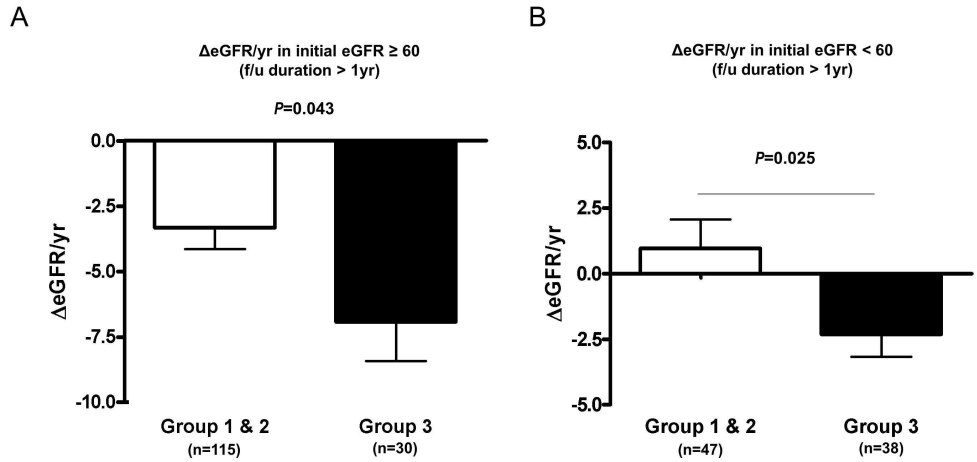

Figure 11. Comparison of ΔeGFR/yr in the two groups (subcategorized by initial eGFR).

We compared annual eGFR decrease (ΔeGFR/year) only in patients who were followed up for more than 1 year. (A) The patients in group 3 showed a rapid decline in renal function both whose initial eGFR $\geq$ 60 ml/min/1.73 m^2 (P = 0.043) and (B) < 60 ml/min/1.73 m^2 (P = 0.025)

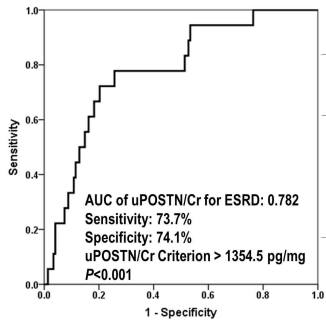

Cut off value (pg/mgCr)	Sensitivity (%)	Specificity (%)	Area	95% CI	
				Upper	Lower
513.0	94.7	46.9	0.782	0.669	0.875
770.8	78.9	59.9			
1354.5	73.7	74.1			
1759.2	68.4	79.6			

Figure 12. ROC analysis and performance in predicting ESRD.

Urinary POSTN/Cr > 1354.5 pg/mgCr demonstrates 74.1% specificity and 73.7% sensitivity in predicting ESRD occurrence. The performance of uPOSTN/Cr at the time of renal biopsy in predicting ESRD is also demonstrated.

Tissue Periostin Expression and Its Correlation with uPOSTN/Cr and Pathologic Findings in IgA Nephropathy

Among the 345 enrolled patients, only 75 unstained slides were available and used for conducting periostin IHC. The correlation between tissue periostin expression and uPOSTN/Cr is demonstrated in Figure 13. Periostin highly stained in patients with high uPOSTN/Cr level (Figure 13A). In morphometry analysis for periostin IHC slides, patients with a high uPOSTN/Cr level showed higher tissue periostin expression (Figure 13B). There was a positive correlation between uPOSTN/Cr and tissue POSTN (r = 0.292; P = 0.011; Figure 13C). On survival analysis for ESRD occurrence by morphometry-result based grouping, ESRD occurred only in patients with high tissue periostin expression (P = 0.003; Figure 13D).

To evaluate the tissue expression of periostin in a human disease model that progressed to fibrosis, we performed Masson's trichrome staining (MTS) and periostin IHC along with a morphometric analysis. The fibrotic area correlated with the increased tissue periostin expression, and the intensity increased with the severity of the IFTA (Figure 14A). The tissue periostin positive area increased with the severity of IFTA and arteriolosclerosis (Figure 14B). The characteristics of the 75 patients who were used in this analysis are shown in Table 4. The tissue periostin values were measured by morphometry and were divided into tertiles, and the three groups were compared. In conclusion, tissue periostin expression was closely associated with a low renal function, tissue IFTA and vessel changes in IgA nephropathy patients.

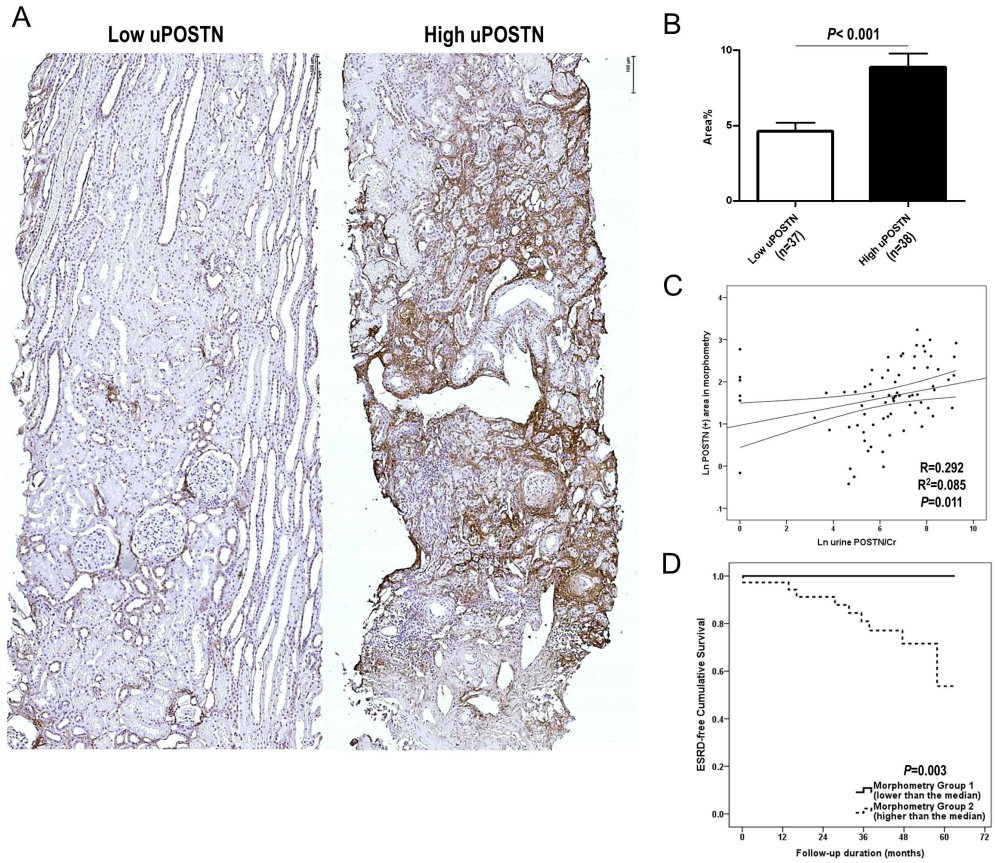

Figure 13. Tissue periostin expression and uPOSTN in IgAN patients.

(A) Periostin immunohistochemistry in IgAN patients (original magnification: × 50) (B) Morphometry results for periostin positive area (%) in uPOSTN two groups (P < 0.001) (C) Correlation between ln-uPOSTN/Cr and morphometry result (r = 0.292, P =0.011)

(D) Kaplan-Meier curve for the occurrence of ESRD according to morphometry positivity area (%) – based grouping (lower than the median value vs. high than the median value). The ESRD occurred only in the patients with high tissue periostin expression (log-rank P = 0.003).

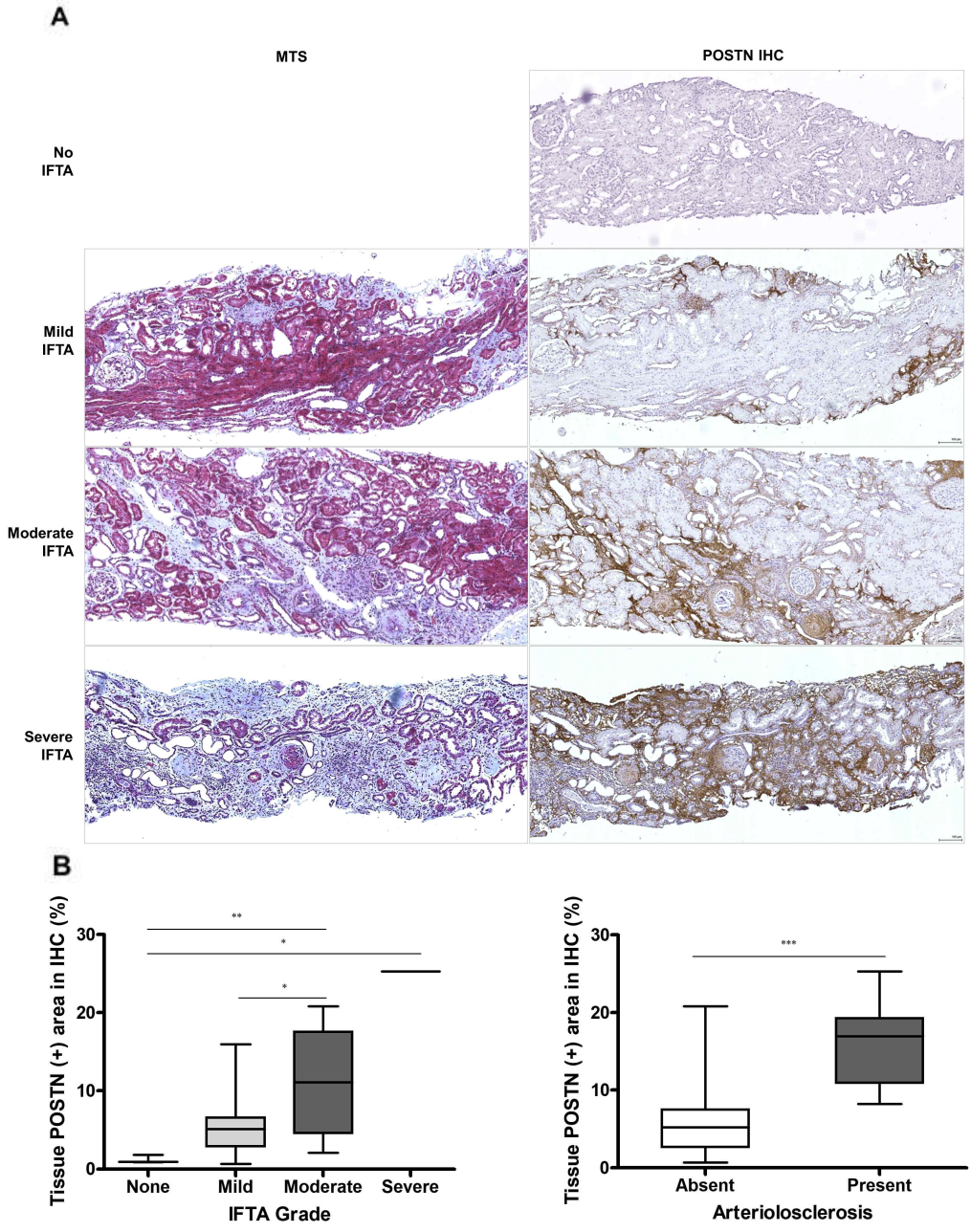
A
MTS
POSTN IHC
No IFTA
Mild IFTA
Moderate IFTA
Severe IFTA
B
Tissue POSTN (+) area in IHC (%)
30
20
10
0
**
*
*
None
Mild
Moderate
Severe
IFTA Grade
Tissue POSTN (+) area in IHC (%)
30
20
10
0
***
Absent
Present
Arteriolosclerosis

Figure 14. Periostin also acts as a fibrosis-related marker in human IgA nephropathy (IgAN) patients

A. Periostin IHC of IgAN patients showed that the fibrotic area correlated with the increased tissue periostin expression, and the intensity increased with the severity of IFTA (original magnification, × 100).

B. When we evaluated a total of 75 IgAN slides, the tissue periostin positivity area increased with the severity of IFTA. Tissue periostin expression also increased in patients with arteriolosclerosis.

(*:$P < 0.05$, **:$P < 0.01$, ***:$P < 0.001$).

Table 4. Clinical characteristics of the 75 IgA nephropathy patients who underwent the morphometric analysis

		Morphometry Tertile Groups*				*P* value
		Group 1 (n = 25)	Group 2 (n = 25)	Group 3 (n = 25)	Total (N = 75)	
uPOSTN/Cr (pg/mL)		975.5±1929.9	982.2±1115.7	2902.0±3149.5	1619.9±2379.4	
Age (year)		38.9±14.8	39.4±12.1	46.0±14.7	41.4±14.1	0.142
Male sex (%)		44.0	40.0	56.0	46.7	0.498
BMI (kg/m^2)		23.4±3.6	22.7±2.9	22.8±3.6	22.9±3.3	0.745
Systolic BP (mmHg)		120.6±12.5	122.0±13.7	134.3±19.2	125.6±16.4	0.005[cd]
Diastolic BP (mmHg)		75.9±11.6	78.0±9.6	85.3±10.5	79.7±11.3	0.008[c]
DM (%)		4.0	4.2	4.2	4.1	0.999
Serum IgA level (mg/dL)		275.5±88.4	272.0±75.8	326.7±94.2	290.9±88.8	0.069
Serum creatinine (mg/dL)		0.97±0.23	1.06±0.29	1.98±1.13	1.34±0.82	<0.001[cd]
IDMS-MDRD eGFR ($mL/min/1.73\ m^2$)		80.6±24.5	71.7±21.9	42.4±21.9	64.9±27.9	<0.001[cd]
Serum albumin (g/dL)		3.9±0.4	4.0±0.3	3.7±0.6	3.9±0.5	0.073
Cholesterol (mg/dL)		183.3±34.3	183.5±28.8	198.3±54.4	188.3±40.7	0.342
Uric acid (mg/dL)		5.8±1.3	5.3±1.2	7.2±1.5	6.1±1.6	<0.001[cd]
hs-CRP (mg/dL)		0.28±0.58	0.10±0.23	0.34±0.83	0.23±0.59	0.393
Spot urine protein/Cr (g/gCr)		1.14±0.96	0.88±0.78	2.67±2.13	1.54±1.59	<0.001[cd]
Patients with spot urine protein/Cr ≥ 1 g/gCr (%)		44.0	20.8	73.9	45.8	0.001
IFTA	Severity (score)[a]	1.00±0.5	1.08±0.28	1.52±0.60	1.18±0.52	0.001[cd]
	Moderate to severe (%)[b]	12.0	8.0	47.7	21.1	0.005
Interstitial Inflammation	Severity (score)[a]	0.96±0.54	1.08±0.40	1.36±0.58	1.13±0.53	0.027[c]
	Moderate to severe (%)	12.0	12.0	40.9	20.8	0.036

Vessel	Fibrointimal thickening (%)	28.0	44.0	88.0	53.3	<0.001
	Hyaline arteriolosclerosis (%)	0.0	0.0	40.0	13.3	<0.001
Segmental sclerosis (mean of %)		5.0±6.1	8.2±9.4	10.2±13.3	7.8±10.1	0.199
Global sclerosis (mean of %)		11.9±10.8	17.4±10.9	43.3±25.9	24.2±22.0	<0.001[cd]
Crescent (mean of %)		0.3±1.1	0.4±1.7	1.6±7.6	0.8±4.5	0.532

Values for the categorical variables are shown as percentages; values for the continuous variables are shown as the means ± standard deviation.

Abbreviations: BMI, body mass index; Cr, creatinine; BP, blood pressure; DM, diabetes mellitus; IDMS, isotope dilution mass spectrometry traceable; eGFR, estimated glomerular filtration rate; CRP, C-reactive protein; IFTA, interstitial fibrosis/tubular atrophy.

[*]The POSTN IHC morphometry results of 75 patients were divided into three groups by tertile values.

[a] The mean value of the severity was calculated as follows: none (0), mild (1, $\leq$ 25%), moderate (2, 26-50%), severe (3, > 50%).

[b] In morphometry tertile group 3, 4 patients were excluded from the analysis due to missing interstitial fibrosis / tubular atrophy information in the pathology readings.

[c] $P < 0.05$, post hoc analysis between groups 1 and 3

[d] $P < 0.05$, post hoc analysis between groups 2 and 3

DISCUSSION

This study shows that periostin production is increased by the induction of fibrosis both *in vitro* and *in vivo*, and fibrosis is potentiated by rPOSTN. The POSTN-KO mice showed a more preserved kidney structure and less fibrous tissue. The integrin αv, β3, and β5 mRNA expression levels were increased by the fibrosis induction, and cell fibrosis was decreased by the RGDS peptide. Moreover, the periostin blockade was performed both *in vitro* and *in vivo* using POSTN-KO mice and the administration of a polyclonal aPOSTNab. Moreover, in biopsy-proved IgA nephropathy patients, a higher uPOSTN/Cr level at renal biopsy is associated with a greater decline in eGFR during follow-up and occurrence of ESRD. Pathologic findings such as IFTA, interstitial inflammation, and hyaline arteriolosclerosis were also related with a high uPOSTN/Cr level. Tissue periostin expression was correlated not only with uPOSTN/Cr but also with the IFTA grades and renal outcome.

TGF-β and its downstream Smad cascade is the most important and well-known pathway in kidney fibrosis, and the administration of a neutralizing antibody against TGF-β showed favorable results in several animal studies.[29-31] However, the use of the TGF-β neutralizing antibody in clinical trials failed to show consistent results and was associated with serious adverse events.[32,33] Although recent studies using TGF-β inhibitors showed an attenuation of kidney fibrosis or a decline in renal function, the abrogation of the anti-inflammatory and anti-tumorigenesis effect of TGF-β signaling is a major concern.[34-37]

Periostin is a nonstructural protein that is considered a new fibrosis marker and has an active role in potentiating fibrosis induction. Periostin is known to be expressed during renal development, but it is not expressed in the normal adult kidney.[38] However, its increased expression has been associated with heart failure, myocardial infarction, muscle injury, asthma and several cancer developments and metastasis.[9-12] Periostin is currently emerging as a marker of and therapeutic target for renal fibrosis, and related studies in various renal diseases have been published recently.[13-19]

Our *in vitro* study results showed that periostin by itself weakly induces fibrosis and mostly potentiates TGF-β-induced fibrosis. Additionally, the POSTN-KO mice showed less fibrosis development, including TGF-β mRNA expression, but a more prominent fibrosis induction than the control group. These results suggest that a dual mechanism is involved in periostin-induced fibrosis via both direct and indirect TGF-β pathways. Previous investigations have shown that TGF-β induces periostin expression,[19,39] and periostin induces proinflammatory cytokines that increase inflammatory cells, which, in turn, produce TGF-β.[40,41] This inflammatory- and fibrotic tissue injury-related vicious cycle impairs kidney construction and function.

Our results showed that the periostin blockade attenuated renal fibrosis by decreasing the inflammatory influx of cytokines and fibrotic signaling. Previous research studies have shown that a decreased periostin expression inhibited TGF-β synthesis,[42] and in a recent investigation of periostin blockade, a protective effect was elicited by blocking TGF-β -pSmad3 signaling and the anti-inflammatory effect.[19] Moreover, the periostin

blockade did not show any type of serious adverse effect in this study. When we combined the results of this study and those reported by previously conducted studies in different organs, periostin emerges as a marker of various organ failures, and its antagonism could be widely applied, but further investigations are needed.

In this experimental study, the impact of periostin on renal fibrosis was more prominent in the *in vivo* model than in the *in vitro* model. In the *in vitro* experiment, the rPOSTN administration resulted in fewer fibrotic changes than the TGF-β treatment. However, when we performed the UUO operation, the mRNA expression levels of fibrosis-related proteins and periostin were minimally increased and were maximally more than 150-fold those in the WT mice. In the POSTN-KO mice, markedly attenuated responses were observed repeatedly. The complicated fibrosis cascade and microenvironments cannot be perfectly reproduced *in vitro*. It appears that the cell-to-cell interaction in tissue and the active communication and crosstalk between the increased ECM and fibrosis-related molecules are important for fibrosis induction and potentiation.

Inflammatory markers showed a tendency that was similar to that of the fibrosis-related markers, i.e., increases in the WT mice and decreases in the POSTN-KO mice. Because fibrosis is an outcome of a failed healing process of inflammation, attenuating the inflammatory process could be an important mechanism for reducing fibrosis in POSTN-KO mice. Various inflammatory cells, such as macrophages, T-lymphocytes, and neutrophils, and related inflammatory cytokines were evenly involved in these processes.

We also examined the expression of p53, which is known to

interact with pSmad3 and other transcriptional cofactors to promote fibrosis in the TGF-β-related cell signaling pathway.[43,44] Previous studies reported that the obstructed kidneys in $p53^{+/-}$ and $p53^{-/-}$ mice exhibited an attenuation of renal tubular and interstitial cell apoptosis compared with those in $p53^{+/+}$ mice.[45] The TUNEL assay showed that apoptosis was decreased in the POSTN-KO mice compared to that in the WT mice, and anti-apoptotic bcl-2 mRNA expression was inversely correlated with p53 and the TUNEL assay.

We antagonized the periostin effect in 3 ways. First, we performed a fibrosis induction and evaluated the fibrosis-related markers similarly in both WT and POSTN-KO mice. Second, we blocked the integrin-binding pathway using RGDS. Third, we used a neutralizing polyclonal aPOSTNab, which was not used in previous studies. All these methods commonly showed an attenuated expression of the fibrosis-related markers compared to those in a positive control group; however, the decreased fibrosis was more prominent in the *in vivo* studies. The aPOSTNab decreased tissue fibrosis, the fibrosis-related mRNA expression, and protein expression. Until recently, a commercial anti-POSTN neutralizing monoclonal antibody (aPOSTNmab) had not been available. The production of and treatment with aPOSTNmab is needed, and it can be a worthy pursuit to identify other therapeutic targets for the treatment of renal fibrosis.

Evidence for periostin as a biomarker in specific renal disease is now emerging.[13,15,17,18,46] However, no previous reports on the association of periostin and IgAN exist, although IgAN is the most common glomerulonephritis worldwide. Our results showing a relation between higher uPOSTN/Cr levels and severe renal fibrosis and poor renal outcomes in

IgAN are consistent with those from previous studies on other renal diseases. We further compared the tissue periostin expression using different IFTA grades and found that the tissue periostin positive area increased with the severity of IFTA. Fibrotic tissue contains periostin, and it can be secreted in urine and detected in the early stage of fibrosis.

Urine POSTN/Cr level was correlated with plasma periostin, but plasma periostin failed to show significant correlations with various other parameters. With regard to renal disease, renal periostin expression has been reported in both glomerulosclerosis and renal tubular fibrosis. Given its nature, serum periostin levels can be affected by systemic conditions in many organs or tissues. However, urine periostin level can be directly affected by local renal tissue periostin expression, especially through tubular secretion. Although we adjusted uPOSTN by urine creatinine level in this study because we considered that every urine sample was diluted differently, only 4 patients were classified into a different group when we used direct uPOSTN level without creatinine adjustment. This finding also shows the possibility that most of the periostin in the urine comes from the tubules. Moreover, uPOSTN/Cr level was well correlated with tissue periostin expression, and tissue periostin expression affected renal outcome. It is difficult to draw a definitive conclusion, as uPOSTN might be mainly pulled by tubular secretion than glomerular filtration.

In IgAN-related research, ESRD is a difficult renal outcome to study because of the takes a long time from diagnosis to onset. However, this study showed a significant difference in the occurrence of ESRD between the lower uPOSTN level group (group 1+2) and the higher

uPOSTN level group (group 3) during the 2.25 years of mean follow-up. This may imply that poor renal outcome is related to baseline characteristics, such as eGFR at the time of renal biopsy. Annual loss of eGFR (ΔeGFR/year) in patients with IgAN is known to vary from -8.4 to 32.3 ml/min/1.73 m^2,[47,48] and the proportion of progression to ESRD is between 6% and 43% over 10 years. Periostin is associated with renal fibrosis, and it would be naturally associated with a decrease in eGFR. To overcome the different follow-up duration and significantly different baseline eGFR between the groups, we divided the patients by initial eGFR (60 ml/min/1.73 m^2)andthencomparedΔeGFR/year between the groups to express and assess the independent effect of periostin on renal outcomes. In this analysis, the commonly high uPOSTN/Cr population had a significantly high ΔeGFR/year. Moreover, when we adjusted for age, sex, uPCr, and serum creatinine at the time of renal biopsy, categorization into group 3 was independently associated with ESRD occurrence.

Because uPOSTN/Cr levels were correlated with tissue periostin expression in various analyses and plasma periostin levels were not correlated with tissue findings, there is a high probability that uPOSTN was excreted from local kidney tissue and reflects the tissue periostin concentration. Finding urinary biomarkers for specific disease entities is useful and has various advantages such as convenient sample collection, highly specificity to local renal expression, and non-invasiveness. Until now, the diagnosis of IgAN is based on histological confirmation, hence urinary biomarkers cannot replace kidney biopsy. There have been many classifications and pathologic staging as efforts to predict the prognosis of

IgAN, and the efforts are continued. These findings, together with those of previous studies reported a correlation between tissue periostin expression and renal fibrosis (especially IFTA), uPOSTN measurement by ELISA is a useful tool to detect tissue periostin expression and to predict renal outcome.

A strength of this study is that all the urine, plasma, and tissue samples were collected at the same time and diagnostic point in each individual disease course. Moreover, as all the patients in this study were included in prospective cohort, researchers were able to collect patients' serial follow-up data after diagnosis. The major limitation of this study is that the ELISA kit was not sensitive enough and the uPOSTN level was too low to be detected. There were 148 patients with an undetectable POSTN level, who were categorized separately into group 1. This made the patients with undetectable uPOSTN level to be excluded in the quantitative analysis such as ROC and this might have caused selection bias. Even though there have been at least 100 articles published about serum POSTN, there are only limited reports about "urine" POSTN. This may be due to the difficulty in detecting uPOSTN using commercially available ELISA kits. In addition, most patients in this study underwent kidney biopsy and were enrolled between 2009 and 2012; therefore, MEST criteria in the Oxford classification could not be applied in the pathologic analysis although we recognize that it offers precise prediction and risk stratification.[49-51] However, the IFTA scoring system used in this study was similar to the MEST criteria, with the same T score, and only endocapillary hypercellularity from the MEST criteria was not included in this study. In the VALIGA study, endocapillary hypercellularity did not predict poor renal outcomes.

Furthermore, in the effect sizes of pathology findings using the MEST criteria, the T score showed the greatest hazard ratio.[50] Furthermore, due to the cross-sectional design of the relationship between uPOSTN/Cr levels and pathologic findings, only associations can be inferred.

In summary, this study identified the role of periostin in renal fibrosis, and its blockade attenuated fibrogenesis in three ways as follows: via the TGF-β signaling pathway, the anti-inflammatory effect, and the anti-apoptotic pathway. To the best of our knowledge, this research study was the first trial to block periostin action by the administration of a daily injection of aPOSTNpab *in vivo*. This study also established a clear relation between high uPOSTN/Cr levels and renal fibrosis, high tissue periostin expression, low eGFR, and rapid decline in renal function in patients with IgAN, the most common glomerulonephritis worldwide. Periostin is a possible early-stage marker for renal fibrosis and a promising urinary biomarker for evaluation of renal fibrosis and prediction of renal outcome in IgAN. In addition, the aPOSTNmab may represent a promising translational opportunity to attenuate many fibrotic diseases.

REFERENCES

1. Y Liu: Renal fibrosis: new insights into the pathogenesis and therapeutics. *Kidney Int* 69: 213-217, 2006.

2. HT Cook: The origin of renal fibroblasts and progression of kidney disease. *Am J Pathol* 176: 22-24, 2010.

3. R Lan, H Geng, AJ Polichnowski, PK Singha, P Saikumar, DG McEwen, KA Griffin, R Koesters, JM Weinberg, AK Bidani, W Kriz, MA Venkatachalam: PTEN loss defines a TGF-beta-induced tubule phenotype of failed differentiation and JNK signaling during renal fibrosis. *Am J Physiol Renal Physiol* 302: F1210-1223, 2012.

4. RL Chevalier: The Proximal Tubule is the Primary Target of Injury and Progression of Kidney Disease: Role of the glomerulotubular junction. *Am J Physiol Renal Physiol*: ajprenal 00164 02016, 2016.

5. MG Kiuchi, D Mion, Jr.: Chronic kidney disease and risk factors responsible for sudden cardiac death: a whiff of hope? *Kidney Res Clin Pract* 35: 3-9, 2016.

6. F Genovese, AA Manresa, DJ Leeming, MA Karsdal, P Boor: The extracellular matrix in the kidney: a source of novel non-invasive biomarkers of kidney fibrosis? *Fibrogenesis Tissue Repair* 7: 4, 2014.

7. A Pozzi, R Zent: Integrins in kidney disease. *J Am Soc Nephrol* 24: 1034-1039, 2013.

8. SJ Conway, K Izuhara, Y Kudo, J Litvin, R Markwald, G Ouyang, JR Arron, CT Holweg, A Kudo: The role of periostin in tissue remodeling

across health and disease. *Cell Mol Life Sci* 71: 1279-1288, 2014.

9. WE Stansfield, NM Andersen, RH Tang, CH Selzman: Periostin is a novel factor in cardiac remodeling after experimental and clinical unloading of the failing heart. *Ann Thorac Surg* 88: 1916-1921, 2009.

10. S Kapoor: Periostin and its emerging role in systemic carcinogenesis. *Osteoporos Int* 25: 1423-1424, 2014.

11. K Ratajczak-Wielgomas, P Dziegiel: The role of periostin in neoplastic processes. *Folia Histochem Cytobiol* 53: 120-132, 2015.

12. C McSharry, S Johnstone: Periostin as a biomarker of airway inflammation. *Pol Arch Med Wewn* 126: 118-120, 2016.

13. B Satirapoj, Y Wang, MP Chamberlin, T Dai, J LaPage, L Phillips, CC Nast, SG Adler: Periostin: novel tissue and urinary biomarker of progressive renal injury induces a coordinated mesenchymal phenotype in tubular cells. *Nephrol Dial Transplant* 27: 2702-2711, 2012.

14. N Braun, K Sen, MD Alscher, P Fritz, M Kimmel, J Morelle, E Goffin, A Jorres, RP Wuthrich, CD Cohen, S Segerer: Periostin: a matricellular protein involved in peritoneal injury during peritoneal dialysis. *Perit Dial Int* 33: 515-528, 2013.

15. B Satirapoj, R Witoon, P Ruangkanchanasetr, P Wantanasiri, M Charoenpitakchai, P Choovichian: Urine periostin as a biomarker of renal injury in chronic allograft nephropathy. *Transplant Proc* 46: 135-140, 2014.

16. DP Wallace, C White, L Savinkova, E Nivens, GA Reif, CS Pinto, A Raman, SC Parnell, SJ Conway, TA Fields: Periostin promotes renal cyst growth and interstitial fibrosis in polycystic kidney disease. *Kidney Int* 85: 845-854, 2014.

17. P Wantanasiri, B Satirapoj, M Charoenpitakchai, P Aramwit: Periostin: a novel tissue biomarker correlates with chronicity index and renal function in lupus nephritis patients. *Lupus* 24: 835-845, 2015.

18. B Satirapoj, S Tassanasorn, M Charoenpitakchai, O Supasyndh: Periostin as a tissue and urinary biomarker of renal injury in type 2 diabetes mellitus. *PLoS One* 10: e0124055, 2015.

19. M Mael-Ainin, A Abed, SJ Conway, JC Dussaule, C Chatziantoniou: Inhibition of periostin expression protects against the development of renal inflammation and fibrosis. *J Am Soc Nephrol* 25: 1724-1736, 2014.

20. RJ Wyatt, BA Julian: IgA nephropathy. *N Engl J Med* 368: 2402-2414, 2013.

21. JH Chang, DK Kim, HW Kim, SY Park, TH Yoo, BS Kim, SW Kang, KH Choi, DS Han, HJ Jeong, HY Lee: Changing prevalence of glomerular diseases in Korean adults: a review of 20 years of experience. *Nephrol Dial Transplant* 24: 2406-2410, 2009.

22. JB Layton, SL Hogan, CE Jennette, B Kenderes, J Krisher, JC Jennette, WM McClellan: Discrepancy between Medical Evidence Form 2728 and renal biopsy for glomerular diseases. *Clin J Am Soc Nephrol* 5: 2046-2052, 2010.

23. H Lee, DK Kim, KH Oh, KW Joo, YS Kim, DW Chae, S Kim, HJ Chin: Mortality of IgA nephropathy patients: a single center experience over 30 years. *PLoS One* 7: e51225, 2012.

24. MA Abdalla, Y Haj-Ahmad: Promising Urinary Protein Biomarkers for the Early Detection of Hepatocellular Carcinoma among High-Risk Hepatitis C Virus Egyptian Patients. *J Cancer* 3: 390-403, 2012.

25. H Rios, SV Koushik, H Wang, J Wang, HM Zhou, A Lindsley, R Rogers, Z Chen, M Maeda, A Kruzynska-Frejtag, JQ Feng, SJ Conway: periostin null mice exhibit dwarfism, incisor enamel defects, and an early-onset periodontal disease-like phenotype. *Mol Cell Biol* 25: 11131-11144, 2005.

26. AB Farris, CD Adams, N Brousaides, PA Della Pelle, AB Collins, E Moradi, RN Smith, PC Grimm, RB Colvin: Morphometric and visual evaluation of fibrosis in renal biopsies. *J Am Soc Nephrol* 22: 176-186, 2011.

27. D Faust, A Geelhaar, B Eisermann, J Eichhorst, B Wiesner, W Rosenthal, E Klussmann: Culturing primary rat inner medullary collecting duct cells. *J Vis Exp*, 2013.

28. KJ Livak, TD Schmittgen: Analysis of relative gene expression data using real-time quantitative PCR and the 2(-Delta Delta C(T)) Method. *Methods* 25: 402-408, 2001.

29. K Sharma, Y Jin, J Guo, FN Ziyadeh: Neutralization of TGF-beta by anti-TGF-beta antibody attenuates kidney hypertrophy and the enhanced extracellular matrix gene expression in STZ-induced diabetic mice. *Diabetes* 45: 522-530, 1996.

30. S Chen, MC Iglesias-de la Cruz, B Jim, SW Hong, M Isono, FN Ziyadeh: Reversibility of established diabetic glomerulopathy by anti-TGF-beta antibodies in db/db mice. *Biochem Biophys Res Commun* 300: 16-22, 2003.

31. A Benigni, C Zoja, D Corna, C Zatelli, S Conti, M Campana, E Gagliardini, D Rottoli, C Zanchi, M Abbate, S Ledbetter, G Remuzzi:

Add-on anti-TGF-beta antibody to ACE inhibitor arrests progressive diabetic nephropathy in the rat. *J Am Soc Nephrol* 14: 1816-1824, 2003.

32. AL Mead, TT Wong, MF Cordeiro, IK Anderson, PT Khaw: Evaluation of anti-TGF-beta2 antibody as a new postoperative anti-scarring agent in glaucoma surgery. *Invest Ophthalmol Vis Sci* 44: 3394-3401, 2003.

33. CP Denton, PA Merkel, DE Furst, D Khanna, P Emery, VM Hsu, N Silliman, J Streisand, J Powell, A Akesson, J Coppock, F Hoogen, A Herrick, MD Mayes, D Veale, J Haas, S Ledbetter, JH Korn, CM Black, JR Seibold, G Cat-192 Study, C Scleroderma Clinical Trials: Recombinant human anti-transforming growth factor beta1 antibody therapy in systemic sclerosis: a multicenter, randomized, placebo-controlled phase I/II trial of CAT-192. *Arthritis Rheum* 56: 323-333, 2007.

34. N Shen, H Lin, T Wu, D Wang, W Wang, H Xie, J Zhang, Z Feng: Inhibition of TGF-beta1-receptor posttranslational core fucosylation attenuates rat renal interstitial fibrosis. *Kidney Int* 84: 64-77, 2013.

35. D Tampe, M Zeisberg: Potential approaches to reverse or repair renal fibrosis. *Nat Rev Nephrol* 10: 226-237, 2014.

36. K Sharma, JH Ix, AV Mathew, M Cho, A Pflueger, SR Dunn, B Francos, S Sharma, B Falkner, TA McGowan, M Donohue, S Ramachandrarao, R Xu, FC Fervenza, JB Kopp: Pirfenidone for diabetic nephropathy. *J Am Soc Nephrol* 22: 1144-1151, 2011.

37. H Trachtman, FC Fervenza, DS Gipson, P Heering, DR Jayne, H Peters, S Rota, G Remuzzi, LC Rump, LK Sellin, JP Heaton, JB Streisand, ML Hard, SR Ledbetter, F Vincenti: A phase 1, single-dose study of fresolimumab, an anti-TGF-beta antibody, in treatment-resistant primary focal

segmental glomerulosclerosis. *Kidney Int* 79: 1236-1243, 2011.

38. T Ito, A Suzuki, E Imai, N Horimoto, T Ohnishi, Y Daikuhara, M Hori: Tornado extraction: a method to enrich and purify RNA from the nephrogenic zone of the neonatal rat kidney. *Kidney Int* 62: 763-769, 2002.

39. K Horiuchi, N Amizuka, S Takeshita, H Takamatsu, M Katsuura, H Ozawa, Y Toyama, LF Bonewald, A Kudo: Identification and characterization of a novel protein, periostin, with restricted expression to periosteum and periodontal ligament and increased expression by transforming growth factor beta. *J Bone Miner Res* 14: 1239-1249, 1999.

40. JT Butcher, RA Norris, S Hoffman, CH Mjaatvedt, RR Markwald: Periostin promotes atrioventricular mesenchyme matrix invasion and remodeling mediated by integrin signaling through Rho/PI 3-kinase. *Dev Biol* 302: 256-266, 2007.

41. SS Sidhu, S Yuan, AL Innes, S Kerr, PG Woodruff, L Hou, SJ Muller, JV Fahy: Roles of epithelial cell-derived periostin in TGF-beta activation, collagen production, and collagen gel elasticity in asthma. *Proc Natl Acad Sci U S A* 107: 14170-14175, 2010.

42. P Snider, RB Hinton, RA Moreno-Rodriguez, J Wang, R Rogers, A Lindsley, F Li, DA Ingram, D Menick, L Field, AB Firulli, JD Molkentin, R Markwald, SJ Conway: Periostin is required for maturation and extracellular matrix stabilization of noncardiomyocyte lineages of the heart. *Circ Res* 102: 752-760, 2008.

43. D Macconi, G Remuzzi, A Benigni: Key fibrogenic mediators: old players. Renin-angiotensin system. *Kidney Int Suppl (2011)* 4: 58-64, 2014.

44. R Samarakoon, AD Dobberfuhl, C Cooley, JM Overstreet, S Patel, R

Goldschmeding, KK Meldrum, PJ Higgins: Induction of renal fibrotic genes by TGF-beta1 requires EGFR activation, p53 and reactive oxygen species. *Cell Signal* 25: 2198-2209, 2013.

45. YJ Choi, L Mendoza, SJ Rha, D Sheikh-Hamad, E Baranowska-Daca, V Nguyen, CW Smith, G Nassar, WN Suki, LD Truong: Role of p53-dependent activation of caspases in chronic obstructive uropathy: evidence from p53 null mutant mice. *J Am Soc Nephrol* 12: 983-992, 2001.

46. DP Wallace, MT Quante, GA Reif, E Nivens, F Ahmed, SJ Hempson, G Blanco, T Yamaguchi: Periostin induces proliferation of human autosomal dominant polycystic kidney cells through alphaV-integrin receptor. *Am J Physiol Renal Physiol* 295: F1463-1471, 2008.

47. SF Shi, SX Wang, L Jiang, JC Lv, LJ Liu, YQ Chen, SN Zhu, G Liu, WZ Zou, H Zhang, HY Wang: Pathologic predictors of renal outcome and therapeutic efficacy in IgA nephropathy: validation of the oxford classification. *Clin J Am Soc Nephrol* 6: 2175-2184, 2011.

48. S Lundberg, AR Qureshi, S Olivecrona, I Gunnarsson, SH Jacobson, TE Larsson: FGF23, albuminuria, and disease progression in patients with chronic IgA nephropathy. *Clin J Am Soc Nephrol* 7: 727-734, 2012.

49. ANN Working Group of the International Ig, S the Renal Pathology, IS Roberts, HT Cook, S Troyanov, CE Alpers, A Amore, J Barratt, F Berthoux, S Bonsib, JA Bruijn, DC Cattran, R Coppo, V D'Agati, G D'Amico, S Emancipator, F Emma, J Feehally, F Ferrario, FC Fervenza, S Florquin, A Fogo, CC Geddes, HJ Groene, M Haas, AM Herzenberg, PA Hill, RJ Hogg, SI Hsu, JC Jennette, K Joh, BA Julian, T Kawamura, FM Lai, LS Li, PK Li, ZH Liu, B Mackinnon, S Mezzano, FP Schena, Y

Tomino, PD Walker, H Wang, JJ Weening, N Yoshikawa, H Zhang: The Oxford classification of IgA nephropathy: pathology definitions, correlations, and reproducibility. *Kidney Int* 76: 546-556, 2009.

50. R Coppo, S Troyanov, S Bellur, D Cattran, HT Cook, J Feehally, IS Roberts, L Morando, R Camilla, V Tesar, S Lunberg, L Gesualdo, F Emma, C Rollino, A Amore, M Praga, S Feriozzi, G Segoloni, A Pani, G Cancarini, M Durlik, E Moggia, G Mazzucco, C Giannakakis, E Honsova, BB Sundelin, AM Di Palma, F Ferrario, E Gutierrez, AM Asunis, J Barratt, R Tardanico, A Perkowska-Ptasinska, VsotE-EIW Group: Validation of the Oxford classification of IgA nephropathy in cohorts with different presentations and treatments. *Kidney Int* 86: 828-836, 2014.

51. SJ Barbour, G Espino-Hernandez, HN Reich, R Coppo, IS Roberts, J Feehally, AM Herzenberg, DC Cattran, Valiga, D Oxford, V North American: The MEST score provides earlier risk prediction in IgA nephropathy. *Kidney Int*, 2015.

국문요약

페리오스틴이 신섬유화와 신기능 저하에 미치는 영향

황진호

의학과 내과학 전공

서울대학교 대학원

서론: 페리오스틴은 인테그린과 상호작용을 함으로써 조직 재생, 섬유화, 창상치유 등에 중요한 역할을 하는 matricellular protein 이다. 최근 페리오스틴이 신장학 영역에서 하는 역할에 대한 관심이 증가하고 있다. 본 연구자는 신장 섬유화 과정에서 페리오스틴을 차단하는 것이 어떤 영향을 미치는지와, IgA 신병증 환자에서 페리오스틴이 지니는 임상적 의의를 연구하였다.

방법: 동물실험으로, 표준형 (wild-type) 마우스와 페리오스틴 결핍 (POSTN-KO) 마우스에서 일측요관폐쇄모델 (UUO)을 만들어 비교함으로써 페리오스틴의 기능을 조사하였다. 생체 외 실험을 위해, wild-type 과 POSTN-KO 마우스에서 각각 초대 배양한 내수질집합관세포 (IMCD cell)를 이용하였다. 인체의 질병과 관련한 연구를 위해서는, 314명의 IgA 신병증 환자에서 혈청과 요의 페리오스틴 농도를 엘라이자 (ELISA)로 측정하였다. 대상 환자들은 요 페리오스틴/크레아티닌 비 (uPOSTN/Cr) 값을 기준으로 다음의 세 그룹으로 분류하였다: 그룹 1 (페리오스틴 불검출군), 그룹 2 (중앙값보다 낮은 페리오스틴 값을 보이

는 군), 그룹 3 (중앙값보다 높은 페리오스틴 값을 보이는 군).

결과: Wild-type 마우스에서 UUO에 의해 페리오스틴이 매우 강력하게 발현되었다. 생체 외 실험에서, wild-type IMCD에 재조합 TGF-β를 투여하여 섬유화를 조장하였을 때 페리오스틴 발현이 증가하였다. 페리오스틴 작용을 세가지 방식으로 차단하여 그 효과를 비교하였다. Wild-type 마우스에 비하여 POSTN-KO 마우스는 신장 조직 구조가 더 잘 보존되었고, 섬유화가 덜 발생하였다. 또한, wild-type 마우스에 비해 POSTN-KO 마우스에서 섬유화 관련 유전자 및 염증성 사이토카인 유전자의 발현이 유의하게 감소하였다. 인테그린 차단 펩타이드와 항페리오스틴 다클론항체의 처리를 통해 섬유화 관련 유전자 발현이 감소되었다. 요의 POSTN/Cr 값은 병리학적 분류 단계, 조직검사 당시의 신기능 및 최종 신기능과 유의한 연관관계를 보였다 (P<0.001). 조직학적으로, 그룹 3의 환자들은 더 심한 간질 섬유화/세뇨관 위축 (P=0.004), 간질 염증 (P=0.007), 유리질 세동맥경화증 (P=0.001) 및 사구체 경화 (P<0.001) 소견을 보였다. 조직검사 당시의 요 POSTN/Cr 값이 높은 경우 추적 관찰동안 더 큰 폭으로 신기능이 감소하였고 (초기 사구체여과율 ≥ 60 mL/min/1.73 m^2일 때 P=0.043; eGFR < 60 mL/min/1.73 m^2 일 때 P=0.025), 신기능 예후를 볼 때 말기신부전 발생 (P=0.003), 말기신부전 또는 사구체여과율 30% 이상 감소 (P=0.033), 말기신부전 또는 사구체여과율 50% 이상 감소 (P=0.046)가 그룹 3의 환자들에서 유의하게 많이 발생하였다. 다변량 분석에서도 요 uPOSTN/Cr 그룹 3인 환자들이 말기신부전 발생 증가와 유의하게 연관되었다 (위험도, 2.839; 신뢰구간, 1.013-7.957; P=0.047).

결론: 페리오스틴은 신장 섬유화의 표지자이자 세포외 물질 단백으로서 섬유화의 진행을 촉진시킨다. 페리오스틴 작용을 차단하면 TGF-β의 신

호전달체계와 염증 및 세포자멸사를 억제함으로써 신장 섬유화를 약화시킨다. 초기 진단 당시 요의 POSTN/Cr 값은 IgA 신병증 환자에서 신장 섬유화의 정도와 연관될 뿐 아니라, 신기능 예후를 예측한다. 본 연구의 결과는, 페리오스틴이 신장 섬유화에 유망한 요 생체표지자일 수 있으며, 페리오스틴의 작용을 차단하는 것이 신장 섬유화를 억제하는 새로운 치료 타겟이 될 수 있다는 가능성을 제시한다.

주요어: 항페리오스틴 항체; 생체표지자; 만성콩팥병; 섬유화; IgA 신병증; 페리오스틴

학번: 2012-30537